THE ASTROPHYSICAL JOURNAL, 283:694–709, 1984 August 15

CONFINEMENT OF THE CRAB PULSAR'S WIND BY ITS SUPERNOVA REMNANT

C. F. KENNEL[1] AND F. V. CORONITI[2]
Received 1983 April 18; accepted 1984 February 29

ABSTRACT

We construct a steady state, spherically symmetric, magnetohydrodynamic model of the Crab nebula. A highly relativistic, positronic pulsar wind is terminated by a strong MHD shock that decelerates the flow and increases its pressure to match boundary conditions imposed by the recently discovered supernova remnant that surrounds the nebula. If the magnetic luminosity of the pulsar wind upstream of the shock is about 0.3% of its particle luminosity, the pressure and velocity boundary conditions imposed by the remnant place the shock where we infer it to be: near the outer boundary of an underluminous region observed to surround the pulsar. It is necessary to include the weak magnetization of the wind to satisfy the boundary conditions and to calculate the nebular synchrotron radiation self-consistently.

Subject headings: nebulae: Crab nebula — nebulae: supernova remnants — plasmas — pulsars — stars: winds

I. INTRODUCTION

The Crab nebula has the longest history of observation of any supernova remnant. It contains the most thoroughly studied pulsar, the only one whose date of birth is known to the year. Despite these singular advantages, the problems in understanding the Crab in terms of other pulsars and remnants have yielded slowly with time. It had seemed that the Crab might be exceptional. Minkowski (1971) suggested its supernova light curve differed from those of both Type I and Type II supernovae. The nebula appears to contain less mass and energy than typical supernova remnants. Detection of the thermal X-ray emissions characteristic of other remants has proven elusive. Its radio spectrum is considerably flatter than that of most remnants. The pulsar is statistically singular, because of its youth, and the system itself is atypical, because it is one of only three remnants known to contain a pulsar. Only recently has it been recognized that the Crab is the defining member of a class of "plerionic" remnants, which possess center-filled radio sources with flat spectra, and, by implication, pulsars (Weiler and Panagia 1978).

There is no generally accepted model which links the pulsar to the nebular synchrotron emission, although one has been sought for the past fifteen years. There is no consensus about how the pulsar's energy output is divided between magnetic dipole radiation and a relativistic stellar wind, or about the composition of the plasma escaping from the pulsar's magnetosphere. Neither observation nor theory has settled where and how the pulsar's wind or wave terminates and comes into pressure balance with the nebula's surroundings. There are no clear X-ray and radio signatures of the shock waves that would signal the interaction of the remnant with the interstellar medium and illuminate the flow and pressure configuration beyond the observable nebula.

Notwithstanding all the above, three facts have been luminously clear virtually since the discovery of the pulsar in 1968. The pulsar's energy output is converted into nebular synchrotron luminosity with an astonishingly high efficiency, 10%–20%. The pulsar also provides the nebula with its magnetic field, which is so strong that it cannot have been primordial field frozen into the expanding nebular flow. The pulsar and nebula therefore form a tightly coupled hydromagnetic system. Finally, the equipartition energy density calculated from synchrotron radio observations leads to a lower limit on the pressure in the nebula that far exceeds that of the interstellar medium. Thus, the pulsar's energy outflow, whatever its form, *is* confined, although until recently the confining material had no obvious observational signature.

A classic paper by Rees and Gunn (1974) outlined an essentially hydrodynamic model of the interaction between the Crab pulsar and nebula which was consistent with the theoretical and observational facts and uncertainties as they stood in 1974. Recent progress in the theory of pair production in pulsar magnetospheres (Cheng and Ruderman 1977; Arons 1979), the suspicion that a strong pulsar wave cannot propagate in the dense pair plasma (Kennel and Pellat 1976; Asseo, Kennel, and Pellat 1978), the development of a theory of hot relativistic stellar winds (Kennel, Fujimura, and Okamoto 1983), and the growing realization that the Crab may have a normal supernova remnant modified by interaction with the pulsar outflow (Chevalier 1977)—together with confirming observations of an extended Hα envelope surrounding the radio nebula (Murdin and Clark 1981)—suggest that reexamination of Rees and Gunn's model might clarify its conceptual basis and render it more quantitative.

The objective of this paper is to develop a self-consistent steady state magnetohydrodynamic model of the flow of relativistic plasma and the magnetic field from the pulsar to the outer boundary of the nebula, where the relativistic flow is confined by the supernova remnant. A self-consistent description of the flow and magnetic field is necessary to calculate the synchrotron radiation from the nebula, a task we undertake in a companion paper (Kennel and Coroniti 1984). There we will find that our steady MHD model can account for the intensity and spatial distribution of the synchrotron radiation, from the infrared to the highest energy γ-rays, but not the radio emissions.

In § II, we will present the observational and theoretical context from which this paper has emerged. In § II*a*, we summarize the implications of recent developments in the theories

[1] Department of Physics, Institute for Geophysics and Planetary Physics, and Center for Plasma Physics and Fusion Engineering, University of California, Los Angeles.
[2] Departments of Physics and Astronomy, University of California, Los Angeles.

of pulsar magnetospheres, relativistic plasma waves, and relativistic stellar winds, as well as review those observations that suggest the existence of a magnetohydrodynamic wind in the nebula. In § II*b*, we repeat Chevalier's (1977) arguments that the Crab may have a normal Type II remnant and review recent observations that support this position. In § III, we will review Rees and Gunn's model and introduce ours, comparing the two at each step. In so doing, we will outline the rest of the paper.

We will refer in the following discussion to Figure 1, which schematically illustrates different regions in the Crab pulsar, nebula, and supernova remnant complex.

II. OBSERVATIONAL AND THEORETICAL BACKGROUND

a) The Pulsar and Nebula

Any theory of the interaction between the Crab pulsar and its nebula must come to grips with certain basic questions of pulsar physics. For example, what kind of plasma, ionic or positronic, charge-separated or quasi-neutral, does the pulsar create in its inner magnetosphere? How is the energy flux streaming from the pulsar to the nebula divided between energetic particles, magnetic field, and large-amplitude waves? Recent theoretical research, we believe, now permits a clear qualitative choice between the alternatives above, though the details of the outflow powered by the pulsar cannot yet be specified quantitatively.

There are strong reasons to believe that pulsars create a pair plasma on the open current-carrying magnetic field lines that connect the polar caps of a magnetized neutron star to its exterior magnetosphere. Sturrock (1971) and Ruderman and Sutherland (1975) argued that pairs can be produced in a small, unsteady vacuum sheath just above a pulsar's polar caps. Fawley, Arons, and Scharlemann (1977), Scharlemann, Arons, and Fawley (1978), Arons and Scharlemann (1979), Scharlemann (1979), Arons (1979, 1981*a*, *b*), and Barnard and Arons (1982) developed a model in which pairs can be produced on favorably curved field lines that connect to the polar caps and bend toward the rotation axis. Following Holloway (1973), Cheng, Ruderman, and Sutherland (1976) and Cheng and Ruderman (1977) suggested that pairs can be produced at "outer gaps" in the distant magnetosphere.

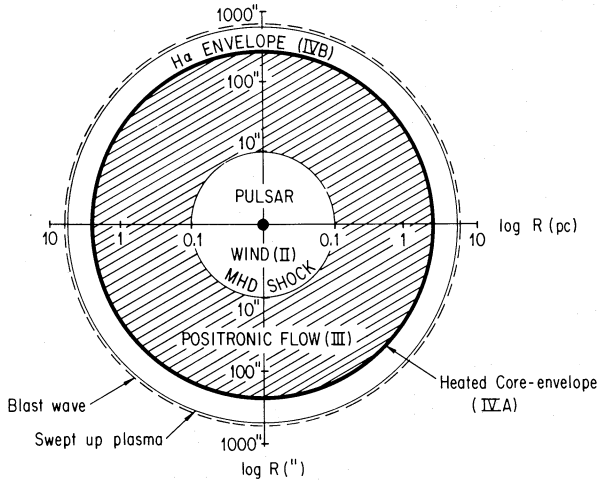

FIG. 1.—*Schematic relation between Crab nebula and supernova remnant.* This figure presents the idealized model of the Crab nebula and supernova remnant whose structure and dimensions underlie our reasoning and computations concerning the positronic flow in the nebula. The dot in the center of the figure represents the Crab pulsar and magnetosphere, within which a hot, relativistic positronic plasma is created. This positronic plasma organizes itself into a reasonably spherically symmetric wind which is contained within the innermost circle of the figure. The wind zone is bounded by a strong MHD shock, whose radial distance from the pulsar we estimate from the observed size of the underluminous zone surrounding the pulsar. The nebula, in our definition, is the region of decelerated positronic flow between the shock, at $r_S = 0.1$ pc, and the inner edge of the supernova remnant, for which we choose an average radius $r_N = 2$ pc. The inner portion of the expanding remnant has been shock heated as a result of its interaction with the pulsar flow. Beyond this is a hydrogenic envelope that was detected by Murdin and Clark (1981) in Hα radiation. The dimensions of the observed envelope indicate it has expanded with a speed of 5000 km s^{-1}. It should have a weak reverse shock at its outer edge and be led by a strong shock propagating into a low-density interstellar medium.

Where in the magnetosphere are pairs created, and how many are created, are questions still not settled. What does seem clear is that pair production provides a background plasma in which coherent radio pulses can be generated, that ions constitute a small fraction of the magnetospheric plasma by number, and that the plasma is charge neutral once it leaves the charge-separated region of pair production near the pulsar. The escaping pair density depends on the number of generations of pairs that are photoproduced and differs from model to model. However, the pair density necessarily exceeds the Goldreich-Julian (1969) charge density, which neutralizes the parallel component of the pulsar's vacuum electric field. This fact has two important theoretical consequences, which we discuss below.

A suggestion that the Crab nebula's optical continuum might be produced by electrons interacting with a strong pulsar wave (Rees 1971*a*; Gunn and Ostriker 1971) led to a prediction, based on a vacuum wave model, of a substantial circular polarization in the optical (Rees 1971*b*; Arons 1972; Blandford 1972). That the required circular polarization was not detected optically (Landstreet and Angel 1971) or at 610 MHz (Weiler 1973; Weiler and Wilson 1977) strictly speaking ruled out only a vacuum pulsar wave in the nebula. The pulsar wave should propagate in a plasma, and the necessary calculations of the circular polarization from the possible strong plasma waves have neither been done nor been compared with observation. Theoretical arguments do suggest that a "superluminous" plasma wave cannot carry the bulk of the pulsar's energy flux. Such a wave cannot propagate near the light cylinder if the plasma density exceeds the Goldreich-Julian density (Max and Perkins 1971; Kennel, Schmidt, and Wilcox 1973; Kennel and Pellat 1976). If the plasma were less dense, so a "superluminous" wave could propagate, the wave would lose all its energy to synchro-Compton radiation after propagating about 10 wavelengths from the Crab pulsar (Asseo, Kennel, and Pellat 1978). Finally, analytic calculation (Max and Perkins 1972; Max 1973) and numerical simulation (Leboeuf *et al.* 1982) both show that a "superluminous" wave near cutoff is violently unstable.

All in all, it appears that if the Crab pulsar is pair-producing, the "superluminous" plasma wave would be suppressed. On the other hand, the pair plasma almost by definition would be dense enough for the magnetohydrodynamic approximation to be valid (Kennel, Fujimura, and Pellat 1979). Thus, the Crab pulsar could generate a relativistic stellar wind. The periodicity due to the misalignment of the pulsar's spin and dipole axes should then modulate the outflow at the pulsar's spin frequency (~ 30 Hz) with a wavelength of about 1.5×10^8 cm. Near the spin equatorial plane, such an outflow would have a small-scale sector structure similar to that of the solar wind.

We now turn to the observational evidence for an MHD flow in the Crab nebula. After that, we review relativistic stellar wind theory as it pertains to the present problem.

Piddington (1957) was the first to suggest that a rapidly rotating magnetized object could fill the Crab nebula with a toroidal magnetic field that is perpendicular to the spin axis of the central rotator. Such a model explains the uniform and strong optical polarization that Woltjer (1957) found near the center of the Crab nebula. It has been obvious since its discovery that the pulsar could create a toroidal field, and numerous measurements at many photon energies have confirmed the existence of a region of quasi-uniform polarization centered on the pulsar (Hogg *et al.* 1969; Wilson 1972; Matveenko 1972; Matveenko and Meeks 1973; Weisskopf *et al.* 1976; Schmidt, Angel, and Beaver 1979; Swinbank and Pooley 1979; Wright and Forster 1980). The polarization vector in the $100'' \times 200''$ region surrounding the pulsar is in virtually the same direction (position angle $\sim 155°$) over a wide range of radio frequencies (Matveenko and Kostenko 1979), in the optical (Woltjer 1957), and at X-ray wavelengths (Weisskopf *et al.* 1976). A high-resolution optical study (Schmidt, Angel, and Beaver 1979) revealed that the toroidal field extends to within 10″–20″ from the pulsar and has no significant spatial structure on scales less than 10″, about the radius of curvature of the magnetic field near the center of the nebula.

A toroidal magnetic field is characteristic of a magnetized stellar wind from a rotating central object, either nonrelativistic (Weber and Davis 1967) or relativistic (Michel 1969). The projection of the Crab pulsar's spin axis on the plane of the sky, which in a wind model is parallel (or antiparallel) to the electric field vector of the synchrotron radiation, appears to be aligned more or less along the long axis of the Crab nebula.

The region immediately surrounding the Crab pulsar is underluminous at radio (Wilson 1972), optical (Woltjer 1957; Shklovsky 1968; Scargle 1971; Schmidt, Angel, and Beaver 1979), and X-ray wavelengths (Wolff *et al.* 1975; Aschenbach and Brinkman 1975; Davison, Culhane, and Morrison 1975; Fukada *et al.* 1975; Ricker *et al.* 1975; Staubert *et al.* 1975; Kestenbaum *et al.* 1975, 1976; Palmieri *et al.* 1975; Ku *et al.* 1976; Makishima *et al.* 1981). Schmidt, Angel, and Beaver's (1979) observations make this point very clearly. The optical surface brightness is about 60% of the maximum surface brightness of the nebula in an approximately $20'' \times 20''$ region centered on the pulsar. After subtraction of foreground and background radiation, the residual surface brightness, which is less than 10% of that outside, is consistent with zero volume emissivity. The projected magnetic field just outside the underluminous region has toroidal symmetry centered on the pulsar. The wisps—small regions of variable optical brightness—appear to lie near the boundary of the underluminous zone (Scargle 1969; Schmidt, Angel, and Beaver 1979). Thus, although it is believed that the Crab pulsar powers the nebular synchrotron radiation, there is no observational manifestation of the enormous energy flux required to flow through the volume enclosing the pulsar.

Any wind flowing from the Crab pulsar is likely to be highly relativistic, especially if it is positronic. Indeed, Wilson and Rees (1978) argued that the Lorentz factor of the flow must exceed 10^4 in order that induced Compton scattering not smear the pulsar's radio pulses. Arons (1983) has pointed out to us that inclusion of the magnetic field in the Compton-scattering calculation could alter the above lower limit to the wind's four speed.

A reverse shock must stand in a confined wind in order to decelerate it to a nonrelativisitic expansion speed. If the wind is highly relativistic, an element of flow will spend much less proper time upstream of the shock than in the decelerated thermalized flow downstream. An exterior observer will therefore find that the volume emissivity is smaller upstream and that radiation is emitted more isotropically downstream of the shock. These arguments made it natural for Rees and Gunn (1974) to associate the underluminous zone surrounding the pulsar with the unshocked pulsar wind.

Now we turn to the status of relativistic stellar wind theory. Although much has been written about pair production in pulsar magnetospheres, and about relativistic stellar winds, much more needs to be written before a self-consistent theory of a pulsar wind with a pair production source can be constructed. Because pair production rates depend on the strengths of the field-aligned currents in the non-MHD pair production zone, which connects to the wind beyond, the pair production rate and wind structure are intimately related. Present wind theories arbitrarily specify MHD flow parameters at one point in a magnetic flux tube and calculate the subsequent evolution of the flow in that flux tube (Michel 1969, 1973*a*, *b*, 1974; Ardavan 1976, 1979, 1981; Okamoto 1978). Given a source distribution, the latitude dependence of the wind can in principle be calculated (Michel 1973*a*; Scharlemann and Wagoner 1973; Okamoto 1978; Ardavan 1979) away from singular regions near the spin axis and equator. It is fair to say, however, that the geometry of pulsar winds is poorly understood. Given a pair production model and a wind geometry, it is possible to estimate the speed and magnetic field of a wind far from a pulsar's magnetosphere (Kennel, Fujimura, and Pellat 1979), without assurance that the estimate is self-consistent. For a simple spherically symmetric wind, Kennel, Fujimura, and Okamoto (1984) surveyed the dependence of finite-temperature adiabatic MHD winds on a wide range of source parameters, to enable wind theory to respond flexibly to the variety of pulsar source models that have been proposed. They find that the zero-temperature approximation used in nearly all pulsar wind theories can be misleading. In particular, the fast MHD Mach number of cold winds is at most unity. A strong reverse shock cannot stand in a cold wind. However, as in the nonrelativistic case (Hartmann and MacGregor 1980), winds that are (relativistically) hot at injection can achieve large fast Mach numbers (Goldreich and Julian 1970; Kennel, Fujimura, and Okamoto 1983). Rees and Gunn's model, and our elaboration of it, require that the wind be created "hot."

In summary, given that pulsars are expected to create a dense pair plasma, it appears that a large-amplitude plasma wave cannot carry a dominant fraction of the Crab pulsar's energy flux toward the nebula, while a magnetohydrodynamic wind certainly can. There is no observational evidence for such a wave, whereas the large-scale structure of the magnetic field in the Crab nebula is consistent with a wind. There is evidence that the wind is shocked at a distance of about 0.1 pc from the pulsar.

b) The Crab Supernova Remnant

Chevalier's (1977) arguments that the Crab may have a normal supernova remnant are best appreciated by first reviewing in more detail the reasons why the Crab nebula has traditionally been viewed as anomalous. From the historical record, Minkowski (1971) concluded that the Crab's supernova light curve differed from those of both Type I and Type II

supernovae. In addition the mass contained in the traditional $4' \times 7'$ optical nebula and its kinetic energy of expansion appear to be unusually low. The line-emitting filaments contain only 1–2 $M_\odot$ (Trimble 1968; Henry and MacAlpine 1982), and the central pulsar contains about 1.4 $M_\odot$, for a total of 3–4 $M_\odot$, substantially below the mass of typical supernova progenitors. Individual filaments have 500–1500 km s^{-1} expansion speeds (Trimble 1968; Wyckoff *et al.* 1976), which are a factor 3 less than those typical of young Type II remnants. The expansion kinetic energy based upon the observed filament speeds and total mass is not more than 5×10^{49} ergs, far less than the 10^{51} ergs released in a typical supernova. Finally, the shell-like radio (Wilson 1972) and X-ray (Gorenstein *et al.* 1982) emissions usually associated with young supernova blast waves have not been detected.

Chevalier (1977) began his proposed revision of the traditional view by noting that the Crab supernova was as luminous at maximum light as a Type II supernova, and that the luminosities of some other Type II supernovae are known to have declined as slowly as the ancient Chinese observations indicate the Crab's to have done. He suggested that, if the Crab had been a Type II supernova, the visible nebula should be surrounded by an expanding hydrogenic stellar envelope that contains most of the mass and energy from the original explosion (outer region IV in Fig. 1). The envelope's mass would be 8–10 $M_\odot$, and its leading edge should expand into the interstellar medium at a speed of about 5000 km s^{-1}, so that its kinetic energy would be about 10^{51} ergs.

Two lines of evidence now support the notion that the Crab was a Type II supernova, in which a massive star's core collapses to neutron star densities, thereby launching a shock which ejects the stellar envelope. If the material in the Crab nebula's filaments was ejected from the interior of the parent star, the filaments' compositions should reflect the dynamics of the explosion and, in the context of model calculations, the progenitor's mass. Arnett (1975) argued that the enriched helium abundance of the filaments is compatible with a stellar core mass of 2.25–4 $M_\odot$, and a total mass of 10–15 $M_\odot$. Recent spectral abundance determinations in numerous filaments showed that carbon and oxygen are not enriched, which suggests that the progenitor's mass was about 8 $M_\odot$ (Davidson *et al.* 1982; Nomoto *et al.* 1982). A dynamical calculation based upon a 10 $M_\odot$ evolved star as a starting point found that only 0.06 $M_\odot$ of heavy core material would be ejected, while 0.5×10^{51} ergs would be deposited in a He-H envelope (Hillebrandt 1982). The above estimates indicate that the parent star's mass exceeded the 3–4 $M_\odot$ detected within the traditional boundaries of the Crab nebula. The missing mass could be contained in an interfilament medium, or in a shell surrounding the radio nebula, or both.

The fact that the filaments' mass is ~80% helium suggests that either the outer layers of the presupernova star were helium-rich, or that an inconspicuous outer shell of hydrogen-rich material does exist (Davidson 1979). Recent observations with a 150 Å filter centered on Hα have revealed a faint $12' \times 28'$ halo enclosing the $4' \times 7'$ traditional nebula (Murdin and Clark 1981). The halo's dimensions are consistent with average expansion speeds, 3600–8400 km s^{-1} based on a distance of 2 kpc, that are more in line with those expected from a Type II supernova remnant. The halo's Hα emission measure is 7 cm^{-6} pc, consistent with Chevalier's (1977) prediction of 5 cm^{-6} pc, which was based upon a fully ionized envelope of 10 $M_\odot$ at a temperature of 1 eV. Murdin and Clark (1981) estimated, to factor 2 accuracy, the mean ion density in the halo to be 1 cm^{-3}, and the halo mass to be 8 $M_\odot$. If the halo were expanding with an average speed of 5000 km s^{-1}, its energy, 2×10^{51} ergs, would be comparable to that of a Type II supernova remnant.

Recent optical and infrared observations tend to confirm the existence of a massive halo that surrounds the region of nebular synchrotron emission. Dennefeld (1983) attributed faint near-IR spectral features to filaments with speeds of +3880 and +4940 km s^{-1}. Synoptic high spatial and spectral resolution measurements of [O III] lines from the Crab nebula showed extended emission to +3600 km s^{-1} and −2400 km s^{-1} beyond the bright outline of the synchrotron nebula (Clark *et al.* 1983). On the other hand, Wilson and Weiler (1982) found no evidence for a radio shell at 610 MHz surrounding the halo. The radio luminosity of the halo might be low if it were propagating into the low-density phase of the interstellar medium.

To explain the composition and formation of the filaments, Chevalier proposed that an elementally enriched, 1–2 $M_\odot$ interior stellar shell had been decelerated to a speed of about 300 km s^{-1} by its interaction with the more massive outer envelope during the early phases of the supernova expansion. The pulsar subsequently accelerated this shell up to the presently observed velocity of the outer filaments. The energy required, about 5×10^{49} ergs, which is compatible with estimates of the young pulsar's spin-down energy loss, presumably was deposited in the first few decades of the pulsar's life. The interface between the pulsar's relativistic outflow and the accelerating shell may have been Rayleigh-Taylor unstable. If, as shell material fragmented and condensed, it decoupled from the shell and pulsar outflow, it would have left behind the train of partially accelerated filaments that has been observed (Trimble 1968). Clark *et al.*'s (1983) [O III] observations suggest that the filaments are contained within a shell-like volume whose inner and outer diameters are 135″ and 340″, respectively. The filamentary speeds at the inner and outer edges are 720 and 1800 km s^{-1}, respectively, relative to the center of the nebula. The filaments are aligned largely, but not exclusively, parallel to the boundaries of the shell. Chevalier suggested that the remaining material that did not condense into filaments has now caught up with the hydrogenic envelope.

If the pulsar wind flows around the filaments and is now interacting directly with the stellar envelope, the flow configuration will involve four shocks, rather than the two expected when the pulsar interaction is absent. A blast wave will propagate into the interstellar medium ahead of the expanding envelope. Murdin and Clark's (1981) measurements suggest that it might be well outside the radio nebula and should be a source of 20–30 keV X-rays. The deceleration of the envelope by momentum transfer to interstellar material swept up by the blast wave will launch a reverse shock into the envelope from its outer edge (McKee 1974). The pulsar interaction will create a forward shock propagating into the envelope from its inner edge and a reverse shock that propagates in the pulsar wind.

A search for the outermost blast wave revealed no thermal X-ray emissions above the *Einstein* sensitivity threshold (Gorenstein *et al.* 1982). This suggests that the stellar envelope is expanding into a low-density interstellar medium. Other evidence supports this contention. The high velocity of the envelope material implied by the size of the Hα halo, and by Dennefeld's Doppler measurements, suggests that the envelope cannot yet have decelerated appreciably. That portion of the halo's Hα surface brightness profile above sky background, which Murdin and Clark (1981) observed with 1′–2′ resolution, shows no evidence of the dense layer that forms just behind the

interface between the envelope and shocked interstellar plasma (Gull 1973, 1975), when the mass swept up by the blast wave exceeds a few percent of the envelope mass. The asymmetry of the traditional nebula, and more pertinently, of the halo, also suggests that mass pickup has been negligible to date. This asymmetry, presumably due to a nonspherical supernova explosion, should be less pronounced if the swept-up mass were comparable to the envelope mass and the remnant had entered the Sedov similarity phase. Finally, in a more speculative vein, we mention van den Bergh's (1970) "jet," a curious feature which, in projection, appears to protrude from the northern outer edge of the traditional nebula. Recent high-resolution optical measurements (Gull and Fesen 1982) reveal it to be a faint, edge-brightened cylinder with astonishingly straight sides. Since it is difficult to understand how such a delicate structure could have withstood the violent passage of the blast wave, it is likely to be beyond the supernova remnant. Blandford *et al.* (1983) suggested that the jet is a long trail of matter left behind by the presupernova star that is occulted by the bright nebula. The dimensions of the trail imply that the interstellar medium a few parsecs from the site of the final supernova explosion was in its hot, low-density phase.

If interstellar mass pickup has been unimportant, both the blast wave and the outer reverse shock will be difficult to detect. Unfortunately, the evidence for a forward envelope shock created by the pulsar interaction is weak. A lunar occultation experiment (Toor, Palmieri, and Seward 1976) did suggest the possible existence of a 500 eV thermal X-ray source surrounding the smaller but more intense synchrotron X-ray source. Its reported luminosity was 4×10^{36} ergs s^{-1}, and, assuming the volume emissivity constant, its occultation time profile was consistent with a spherical source of $200'' = 2$ pc radius. Charles and Culhane (1977), applying an algebraic reconstruction technique to *Copernicus* X-ray telescope data, found two significant 0.5–1.5 keV X-ray emitting regions, one about 240″ north, and the other about 180″ south, of the pulsar. Both sets of observations suggest that these soft X-rays might come from near the inner boundary, and not the outer edge, of the supernova envelope. However, it is not clear whether the 500 eV X-rays arise wholly from a thermal source, or whether some or all are synchrotron X-rays that have been scattered by interstellar grains (Toor, Palmieri, and Seward 1976). Furthermore, a failure to detect X-ray lines appears to rule out a thermal X-ray source with a luminosity as high as 4×10^{36} ergs s^{-1} (Schattenburg *et al.* 1980).

In closing, we emphasize that the difficulties encountered in detecting three of the four expected shocks are disappointing but not conclusive. The fact that the relativistic plasma in the Crab has a high pressure, and quite probably the fourth (reverse) shock, suggests that all three of the other shocks are present. Their detection would provide valuable information about the density of the interstellar medium surrounding the supernova envelope; the density, temperature, and composition of the envelope; the dynamics of the pulsar wind; and the evolutionary history of the Crab nebula and remnant. Indeed, interpreting the boundary of the underluminous zone as the pulsar wind reverse shock reveals much about the wind, as Rees and Gunn (1974) argued, and we will confirm.

III. MODELING THE CRAB NEBULA

a) Rees and Gunn's Model

Rees and Gunn (1974) idealized the Crab nebula as a roughly spherical cavity of radius r_N, mainly empty except for relativistic particles and electromagnetic fields, whose electrically conducting outer boundary expands with a uniform speed $\dot{r}_N \approx 1500$ km s^{-1}. They divided the pulsar's energy outflow into wind and wave luminosities, with an unspecified ratio between them, and subdivided the wind's luminosity into Poynting flux and particle energy flux, with the ratio σ between the two a free parameter that they constrained using consistency arguments. They estimated that the relativistic Lorentz factor of the wind is between 10^4 and 10^9; later Wilson and Rees (1978) argued that it must exceed 10^4.

Rees and Gunn (1974) pointed out that the supersonic wind (Region II of Fig. 1) would terminate in a standing reverse shock located at a distance r_S from the pulsar. Beyond the shock (Region III), communication with the nebular boundary at r_N via sound waves would adjust the subsonic flow speed to match the expansion speed $\dot{r}_N$ at the boundary of the nebula. They also suggested that the pulsar wave might be absorbed at or slightly beyond the shock, thereby increasing the downstream plasma energy density and pressure by an unknown amount. Kundt and Krotschek (1980) modified this basic picture by arguing that the pulsar waves would be multiply and diffusely reflected at the nebula boundary, thereby filling the cavity with radiation whose pressure greatly exceeds the particle and magnetic pressure of the wind.

By balancing the ram pressure associated with the pulsar's present luminosity against the pressure in the outer nebula inferred from the rate of energy accumulation over the pulsar's lifetime, Rees and Gunn (1974) estimated r_S to be 3×10^{17} cm, or about 10″ for a 2 kpc distance to the nebula. They suggested that the wind zone (Region II) corresponds to the underluminous region surrounding the pulsar, and that the shock might be associated with the optical wisps (Scargle 1969). Rees and Gunn (1974) assumed that the particle pressure greatly exceeded the magnetic pressure downstream of the shock, so that the postshock flow was basically hydrodynamic. A subsonic hydrodynamic flow must be nearly isobaric, and its flow speed will decrease as r^{-2} with increasing radial distance until it matches the nebula's expansion velocity at r_N. Conservation of magnetic flux requires that the strength of the field accumulating in the nebula increase linearly with r until the magnetic and particle pressures become comparable. For Rees and Gunn's (1974) hydrodynamic considerations to be completely consistent, equipartition of field and particle pressures should occur no closer than r_N. The inverse square velocity scaling and flux conservation combine to yield $\sigma \approx (r_S/r_N)^2 \approx 10^{-2}$ when equipartition is achieved at r_N. However, since they found it hard to reconcile the observed brightness profile across the nebula with a field increasing as r all the way out to r_N, they argued that σ is probably in the range 10^{-1} to 10^{-2}.

Although no pulsar source model has succeeded in calculating the ratio of electromagnetic to particle energy fluxes leaving the pulsar's magnetosphere, the conclusion that σ is appreciably less than unity seems at first glance to be counterintuitive. After all, pairs are thought to be produced in superstrong magnetic fields; moreover, a small σ could imply that the Crab pulsar converts its spin-down luminosity into pair energy with an efficiency exceeding any that has been estimated thus far in the literature. Therefore, it will be important to examine the reasoning leading to the estimate of σ with great care.

b) Outline of Present Model and §§ IV, V, *and* VI

In Figure 1, we sketch the idealized working model of the Crab nebula that we have adopted on the combination of

observational and theoretical grounds summarized in § II. Radial distances are estimated assuming a 2 kpc distance to the pulsar, and the distance scale in Figure 1 is logarithmic, given in parsecs and arc seconds on the horizontal and vertical axes, respectively. The flow has been divided into six regions:

Region I: Inside the pulsar magnetosphere, where pairs are produced.

Region II: Beyond the pulsar light cylinder ($r > r_L = 1.5 \times 10^8$ cm), where a highly relativistic wind flows toward the nebula.

Region III: The nebula proper, which contains a positronic flow that has been decelerated and heated by an MHD reverse shock at $r_S \approx 3 \times 10^{17}$ cm = 0.1 pc. Nearly all the nebula's radio, optical, and X-ray synchrotron radiation is generated in Region III, $r_S < r < r_N \approx 2$ pc.

Region IV: The remnant, which has two parts: an inner region that was shock heated because of its interaction with the pulsar, and a surrounding cooler hydrogenic envelope. A weak reverse shock (McKee 1974) should propagate inward from the outer boundary of Region IV, $r \approx 5$ pc.

Region V: Contains the small amount of material that has been swept up by the outward-propagating blast wave ($r \approx 5$ pc).

Region VI: The interstellar medium.

The boundaries separating Regions III and IV and Regions IV and V are neither ideally thin nor regular, as we assumed in drawing Figure 1. For example, the Region III-IV interface may have been unstable to the formation of filaments (Chevalier 1977). Thus, occlusion of ionic matter are really embedded within the "mainly empty cavity," in Region III.

This paper describes the physics of, and the interactions between, Regions II, III, and IV. We will assume that a wind whose luminosity L equals the observed rotational energy loss rate of the Crab pulsar is generated in Region I and achieves highly relativistic speeds in Region II. We need not specify the Lorentz factor of the wind here, other than to require it to be sufficiently large that we can consider the reverse shock to be strong. Comparison of the synchrotron radiation from the postshock flow with observations can fix the wind's Lorentz factor, and the high efficiency with which the pulsar luminosity is converted to nebular luminosity favors a positronic flow. We will neglect the energy flux of any pulsar waves that exist ahead of the shock. The ratio σ of the wind's magnetic to particle energy fluxes can be determined by neither observation nor theory, and we will consider it a constrainable free parameter. In § IV, we will calculate the relativistic Rankine-Hugoniot relations for the strong magnetohydrodynamic shock that separates Regions II and III, paying special attention to the dependence of the jump conditions on σ. The limit $\sigma \rightarrow 0$ retrieves the hydrodynamic result used by Rees and Gunn (1974), and $\sigma > 1$ describes a highly magnetized flow. Only when $\sigma \lesssim 0.1$ can a significant fraction of the wind luminosity be converted into thermal energy and subsequently into synchrotron luminosity.

Rees and Gunn (1974) explicitly allowed for the evolution of the pulsar's luminosity; however, in view of the possibly complex history of the nebula, we will concentrate on the present state of the wind, which can be better defined by observation. In § V, we will calculate the family of *steady state* flow solutions pertinent to Region III. Given the wind luminosity L, these are characterized by two parameters, the radius of the shock, r_S, and σ, both of which can be found by application of flow and pressure conditions at the nebula-remnant interface, $r = r_N$. In § VI, we consider the extent to which these boundary conditions can be defined by present observations. Estimates of the flow speed can be obtained from the size and age of the nebula, from the speeds of the filaments near $r = r_N$, and from the Doppler velocities of remnant spectral lines. The pressure in the outer nebula can only be bounded at present. The equipartition energy density calculated from radio synchrotron observations sets a lower bound on the average pressure which is consistent with the upper bound on the remnant pressure near r_N that is derivable from the failure to detect X-ray lines (Schattenberg *et al.* 1980). Despite these uncertainties, it appears that a Region III solution which is consistent with these boundary conditions and present observations can exist. We will confirm Rees and Gunn's (1974) conclusion that σ must be small, and we will find that σ may need to be 10^{-2}, or less.

c) *Discussion of Assumptions*

We will assume, as did Rees and Gunn (1974), that at present the nebular plasma flows around the filaments with a negligible interaction so far as the gross properties of the flow are concerned. This assumption is motivated by the facts that the magnetic field carried by the nebular flow is observed to be wrapped around the filaments (Wilson 1972), and that the synchrotron radio spectrum does not change near the filaments (Swinbank 1980). Should the present filament-flow interaction be significant, our flow solutions will need to be amended.

We will assume that the postshock flow is adiabatic, whereas in fact it loses internal energy to synchrotron radiation. However, for typical neutron star moments of inertia, the nebula's observed luminosity is 10%–20% of the pulsar's spin-down luminosity (Ruderman 1972), so that the adiabatic assumption is a reasonable first approximation for the present flow, though it may well be inappropriate for the past flow.

Finally, our assumptions of time independence and spherical symmetry merit further discussion. In magnetohydrodynamic flows, pressure imbalances are rectified by the propagation of fast MHD waves, whose speeds always exceed that of sound and approach the speed of light when the magnetic pressure is larger than the plasma energy density. Since the tenuous positronic plasma is relativistic, its sound speed is $c\sqrt{3}$ throughout Region III, so that a fast wave can cross the nebula in 10 yr or less. Thus, we expect the nebular flow to adjust its pressure distribution quasi-statically to the slow changes in its boundary conditions due to the declining luminosity of the pulsar and the expansion of the supernova remnant. A flow solution that is approximately independent of time should in principle be possible, and the moving variations in optical luminosity on wave propagation time scales noted by Scargle (1969) and others may reflect the nebula's effort to adjust to a steady state.

The Crab pulsar has a proper motion of order 100–150 km s^{-1} that is more or less parallel to the long axis of the nebula and the inferred projected spin axis of the pulsar (Trimble 1971; Wyckoff and Murray 1977; Wyckoff *et al.* 1976). The proper motion leads to a small asymmetry in the pressure confining the pulsar wind, which we can neglect. More importantly, one does not expect the pulsar wind itself to be spherically symmetric. Pair production models and stellar wind theory both suggest that the outflows along the spin axis and rotational equator, where the magnetic field must reverse, will differ. Finally, the nebula is observed to be anisotropic. The hard X-rays from the Crab nebula are clearly not spherically distributed (Makishima *et al.* 1981); there is a significant north-

south asymmetry in the optical and soft X-ray luminosities; and the radio nebula is a prolate spheroid, not a sphere. However, the assumption of spherical symmetry is made because it renders the flow equations one-dimensional and easily integrable.

IV. SUPERRELATIVISTIC MAGNETOHYDRODYNAMIC SHOCK

Let us divide the Crab pulsar's spin-down luminosity L just ahead of the shock between particle and magnetic luminosity as follows:

$$L = 4\pi n\gamma u r_S^2 mc^3(1+\sigma)\,, \tag{4.1}$$

where n is the proper density, u is the radial four speed of the flow, $\gamma^2 = 1 + u^2$, r_S is the radial distance of the shock from the pulsar, m is the electron mass, c is the speed of light, σ is the ratio of the magnetic plus electric energy flux to the particle energy flux,

$$\sigma = \frac{B^2}{4\pi nu\gamma mc^2}\,, \tag{4.2}$$

and B is the observer frame magnetic field.

Several important physical statements are implicit in the form of equation (4.1). We assumed that the magnetic field is almost exactly toroidal far from the pulsar—a general feature of the asymptotic limit of relativistic wind theories and very likely an excellent approximation, since the shock is inferred to be 2×10^9 light cylinder radii from the pulsar. We neglected the azimuthal and latitudinal components of the flow velocity for a similar reason. Furthermore, we assumed that the wind's pressure is negligible relative to its dynamic and magnetic pressures ahead of the shock. However, if the wind had a finite pressure at its source, a strong shock can stand in the wind (Kennel, Fujimura, and Okamoto 1983). If the magnetic field is toroidal, the shock will propagate perpendicular to the magnetic field, and if the wind is positronic, it will be superrelativistic upstream of the shock. These two approximations reduce its Rankine-Hugoniot relations to a remarkably simple form that clearly illustrates the dependence of the downstream flow state on σ. Moreover, the jump conditions and the postshock flow solutions to be derived in § V will be independent of the upstream flow speed u_1, so long as u_1 is large.

We will assume that the shock is stationary relative to the pulsar and the observer. In order to change the results derived below significantly, the shock would have to propagate at relativistic speeds, in which case the underluminous zone would change its size on time scales of less than a year, which appears contrary to observation.

Let us now review the derivation of the Rankine-Hugoniot relations for 90° shocks, which emerge as solutions of the following MHD conservation laws:

$$n_1 u_1 = n_2 u_2\,, \tag{4.3}$$

$$E = \frac{u_1 B_1}{\gamma_1} = \frac{u_2 B_2}{\gamma_2}\,, \tag{4.4}$$

$$\gamma_1\mu_1 + \frac{EB_1}{4\pi n_1 u_1} = \gamma_2\mu_2 + \frac{EB_2}{4\pi n_1 u_1}\,, \tag{4.5}$$

$$\mu_1 u_1 + \frac{P_1}{n_1 u_1} + \frac{B_1^2}{8\pi n_1 u_1} = \mu_2 u_2 + \frac{P_2}{n_1 u_1} + \frac{B_2^2}{8\pi n_1 u_1}\,. \tag{4.6}$$

Equation (4.3) has already been used to derive equations (4.5) and (4.6) from the general expressions for the conservation of energy and momentum fluxes. Subscripts 1 and 2 label upstream (Region II) and downstream (Region III) parameters, respectively. The shock frame number density $N = \gamma n$, and B and E denote the shock frame magnetic and electric fields, respectively; μ is the specific enthalpy, which for a gas with an adiabatic index Γ is defined by

$$\mu = mc^2 + \frac{\Gamma}{\Gamma - 1}\left(\frac{P}{n}\right); \tag{4.7}$$

Y, the ratio of shock frame magnetic fields or densities, is given by

$$Y \equiv \frac{B_2}{B_1} = \frac{N_2}{N_1} = \frac{\gamma_2 u_1}{\gamma_1 u_2}\,. \tag{4.8}$$

Solving equation (4.5) for μ_2 and inserting the resulting expression into equation (4.6) leads to

$$Y^2 - Y\left[\frac{2}{\gamma_2 u_2}\left(u_2^2 + \frac{1}{4}\right)\frac{u_1}{\gamma_1}\right] + \left[\frac{2}{\gamma_2 u_2}\left(u_2^2 + \frac{1}{4}\right)\left(\frac{4\pi n_1\mu_1\gamma_1^2}{B_1^2} + \frac{u_1}{\gamma_1}\right)\right] - \frac{2\pi n_1 mc^2}{B_1^2}\frac{u_2}{u_1} - \left(1 + \frac{8\pi n_1\mu_1 u_1^2 + P_1}{B_1^2}\right) = 0\,. \tag{4.9}$$

We made the first of our strong shock approximations in equation (4.9) by assuming that $P_2/n_2 mc^2 \gg 1$ so that $\Gamma_2 = 4/3$. Equations (4.8) and (4.9), together with $\gamma^2 = 1 + u^2$, constitute the Rankine-Hugoniot relations. Continuing further, we assume that P_1 and u_2/u_1 are small, and that $u_1/\gamma_1 \approx 1$, whereupon equation (4.4) reduces to equation (4.10) below, after use of the relation $\gamma_2^2 = 1 + u_2^2$ and the definition $\sigma = B_1^2/4\pi n_1 u_1^2 mc^2$:

$$u_2^2\left(u_2^2 + \frac{1}{4}\right)^2 = (1 + u_2^2)\left(u_2^2 - \frac{1}{4}\frac{\sigma}{1+\sigma}\right)^2\,. \tag{4.10}$$

Since the terms in u_2^6 cancel, equation (4.10) is a biquadratic in u_2 whose solutions are given by

$$u_2^2 = \frac{8\sigma^2 + 10\sigma + 1}{16(\sigma+1)} \pm \frac{1}{16(\sigma+1)}\left[64\sigma^2(\sigma+1)^2 + 20\sigma(\sigma+1) + 1\right]^{1/2}\,. \tag{4.11}$$

The downstream pressure P_2 and temperature T_2 depend upon u_2 as follows:

$$\frac{P_2}{n_1 mc^2 u_1^2} = \frac{1}{4u_2\gamma_2}\left[1 + \sigma\left(1 - \frac{\gamma_2}{u_2}\right)\right], \tag{4.12}$$

$$\frac{T_2}{u_1 mc^2} = \frac{P_2}{n_2 u_1 mc^2} = \frac{1}{4\gamma_2}\left[1 + \sigma\left(1 - \frac{\gamma_2}{u_2}\right)\right], \tag{4.13}$$

and $B_2/B_1 = N_2/N_1 = \gamma_2/u_2$. The solution with the negative sign in equation (4.11) is extraneous because it leads to negative downstream pressure.

The downstream flow speed, the magnetic field and density ratios, and the downstream pressure and temperature (normalized to the upstream dynamic pressure and flow energy per particle, respectively) depend only upon σ in the strong shock approximation. Inspection of the large- and small-σ

limits of equations (4.11)–(4.13) reveals highly contrasting behavior. When σ is large,

$$u_2^2 = \sigma + \frac{1}{8} + \frac{1}{64\sigma} + \cdots , \tag{4.14a}$$

$$\gamma_2^2 = \sigma + \frac{9}{8} + \frac{1}{64\sigma} + \cdots , \tag{4.14b}$$

$$\frac{B_2}{B_1} = \frac{N_2}{N_1} = 1 + \frac{1}{2\sigma} + \cdots , \tag{4.14c}$$

$$\frac{T_2}{u_1 mc^2} = \frac{1}{8\sqrt{\sigma}}\left(1 - \frac{19}{64\sigma}\right) + \cdots . \tag{4.14d}$$

(Note that u_1 must exceed $8\sqrt{\sigma}$ for the strong shock limit to be valid.) Similar calculations show that the downstream magnetic field, dynamic, and particle pressures have the relative ratios $1 : 1/2\sigma : 1/8\sigma^2$. When σ is small,

$$u_2^2 = \frac{1 + 9\sigma}{8} , \tag{4.15a}$$

$$\gamma_2^2 = \frac{9 + 9\sigma}{8} , \tag{4.15b}$$

$$\frac{T_2}{u_1 mc^2} = \frac{1}{\sqrt{18}}(1 - 2\sigma) , \tag{4.15c}$$

$$\frac{B_2}{B_1} = \frac{N_2}{N_1} = 3(1 - 4\sigma) , \tag{4.15d}$$

Equation (4.15a) indicates that the small-σ approximation is valid only for σ less than 0.1. In the limit $\sigma \rightarrow 0$, the downstream three speed u_2/γ_2 approaches $\frac{1}{3}$, B_2/B_1 and N_2/N_1 approach 3, and the particle pressure P_2 and the dynamic pressure Π_2 approach

$$\frac{P_2}{n_1 mc^2 u_1^2} = \frac{2}{3} , \quad \frac{\Pi_2}{n_1 mc^2 u_1^2} = \frac{1}{3} , \tag{4.15e}$$

which are the classical results for a strong, relativistic, hydrodynamic shock.

The Rankine-Hugoniot solutions pass smoothly from the small-σ to the large-σ limits, as is illustrated in Figure 2, which plots the dependence upon σ of the downstream particle, dynamic, and magnetic pressures, all normalized to the total upstream energy density. Other features of the Rankine-Hugoniot solutions will be displayed in Figures 3 and 4.

In summary, large-σ shocks are effectively weak. Although there can be a large change in flow four speed across the shock, the downstream flow speed $u_2 = \sqrt{\sigma}$ is still relativistic, and the three speeds on both sides of the shock are close to the speed of light. Consequently, the shock frame density and magnetic field jumps are small, and the magnetic pressure still dominates downstream. In effect, nearly all the energy dissipation permitted by the Rankine-Hugoniot relations is used up in making the small magnetic field increase required by the conservation of magnetic flux. On the other hand, when σ is small, MHD strong shocks approach the classical hydrodynamic limit. Only when $\sigma \lesssim 0.1$ can a significant fraction of the total energy flux upstream be converted into thermal energy downstream and thereafter into synchrotron luminosity.

Having calculated the flow parameters just downstream of the shock, we now turn to the flow solutions in the nebula (Region III). These too will have a simple yet crucial dependence on σ.

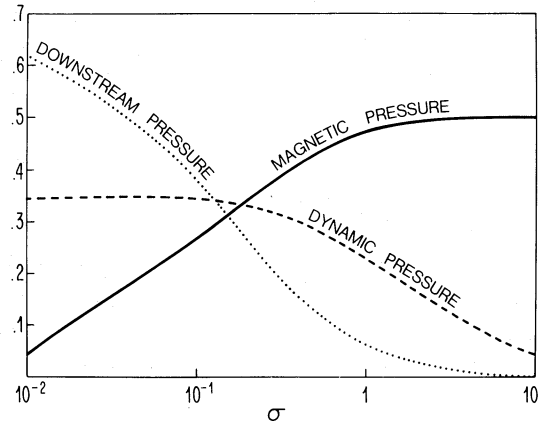

FIG. 2.—*Rankine-Hugoniot solutions for strong relativistic MHD shocks.* This figure plots the dependence of the downstream particle, dynamic, and magnetic pressures, all normalized to the total upstream energy density, as a function of σ, calculated from the Rankine-Hugoniot relations for strong perpendicular shocks. Only when σ is small can most of the upstream particle energy density be converted into thermal energy density downstream. This suggests that low-σ shocks can most efficiently convert wind luminosity into synchrotron luminosity. Other features of the Rankine-Hugoniot solutions are displayed in Figs. 3 and 4.

V. NEBULAR FLOW

a) Basic Equations

The toroidal field approximation we used to such advantage in the derivation of the Rankine-Hugoniot relations also simplified the description of the flow in the nebula. Holzer (1972) used the toroidal approximation in his treatment of the terminations of the solar wind by the interstellar medium; the relativisitic version of this problem presented here is simpler, because all the flow differential equations integrate to a single algebraic equation. Of course, we pay a price to gain this simplicity. The toroidal approximation loses the physics associated with the intermediate and slow wave characteristics. However, we expect these waves to propagate so slowly that they do not affect the flow dynamics on the fast wave time scale.

The steady state equations in the toroidal approximation are: one describing the conservation of number flux,

$$\frac{d}{dr}(cnur^2) = 0 ; \tag{5.1}$$

one describing the conservation of magnetic flux in the magnetohydrodynamic approximation,

$$\nabla \times \left(\frac{\boldsymbol{u} \times \boldsymbol{B}}{\gamma}\right) = 0 \rightarrow \frac{d}{dr}\left(\frac{ruB}{\gamma}\right) = 0 ; \tag{5.2}$$

one describing the propagation of internal energy,

$$\frac{d}{dr}(nur^2 e) + P\frac{d}{dr}(r^2 u) = 0 , \tag{5.3}$$

where e is the relativistic internal energy per particle; and one describing the conservation of total energy,

$$u\frac{d}{dr}(\gamma\epsilon) \equiv \frac{d}{dr}\left[nur^2\left(\gamma\mu + \frac{B^2}{4\pi n\gamma}\right)\right] = 0 , \tag{5.4}$$

where $\mu = e + p$, the specific enthalpy, and ϵ is the total electromagnetic plus particle energy per particle in the proper frame,

$$\epsilon = \mu + \frac{B^2}{4\pi n \gamma^2} . \tag{5.5}$$

By multiplying the radial momentum equation (not shown) by u, and using the adiabatic assumption, $dP/dr = 1/n(d\mu/dr)$, together with $\gamma^2 = 1 + u^2$, we may demonstrate that the radial momentum and total energy equations are equivalent. Maxwell's equations and an equation of state, $P = P(e)$, complete the set of equations. For an isotropic, relativistically hot plasma, $3P = n(e - mc^2)$, which reduces equation (5.3) to

$$\frac{d}{dr} \ln \left(\frac{P}{n^{4/3}} \right) = 0 , \tag{5.6}$$

the equation of state for a relativistic gas with polytropic index 4/3, which we will use henceforth.

We may find the flow solutions from the condition $\gamma\epsilon$ constant implied by equation (5.5). We specify all parameters just downstream of the shock and normalize four speeds and distances to the postshock speed u_2 and shock position r_S, respectively, by defining $z = r/r_S$ and $v = u/u_2$. Then, inserting equations (5.6) and (5.2) into equation (5.4) and integrating leads to the following algebraic equation for the dependence of v upon z:

$$(1 + u_2^2 v^2)^{1/2} \left[\delta + \Delta (vz^2)^{-1/3} + \frac{1}{v} \right] = \gamma_2 (1 + \delta + \Delta) , \tag{5.7}$$

where we define the parameters δ and Δ below, first in terms of postshock quantities and then partially in terms of upstream quantities by using the strong shock jump conditions. We note that

$$\delta = \frac{4\pi n_2 \gamma_2^2 mc^2}{B_2^2} \approx \frac{u_2}{u_1 \sigma} , \tag{5.7a}$$

and that it is small in the strong shock limit and may be neglected. The remaining parameter,

$$\Delta \equiv \frac{16\pi P_2 \gamma_2^2}{B_2^2} = \left(\frac{1 + \sigma}{\sigma} \right) \frac{u_2}{\gamma_2} - 1 , \tag{5.7b}$$

is related to the Alfvén four speed U_{A2} downstream of the shock, since in a relativistically hot plasma with $\Gamma = 4/3$,

$$U_{A2}^2 \equiv \frac{B^2}{4\pi n_2 \gamma_2^2 \mu_2} \approx \frac{1}{\Delta} . \tag{5.7c}$$

Another expression for Δ may be obtained using equation (4.10):

$$\Delta = \frac{(u_2^2/\sigma) - 1/2}{(u_2^2 + 1/4)} . \tag{5.7d}$$

It may be shown, by using either equations (5.7b) or (5.7d), that $\Delta \approx \frac{1}{3}\sigma$ when σ is small, and $\Delta \approx \frac{1}{2}\sigma$ when σ is large. Thus, although Δ passes from large to small values when σ increases, the functional dependence of Δ upon σ hardly changes.

In the strong shock limit, when we may neglect δ, the nebular flow four speed, $u = u_2 v(z)$, depends only on σ (because u_2 and Δ depend only on σ) and r_S (through $z = r/r_S$). To calculate the magnetic or particle pressures, we must also specify the wind luminosity L. We now describe the properties of the solutions to equations (5.7). We first discuss its asymptotic solutions and then its solutions in the $\sigma \gg 1$ and $\sigma \ll 1$ approximations.

b) *Asymptotic Limit*

Let us assume that v remains finite as z tends to infinity. Then, neglecting δ and setting $z \to \infty$ in the term involving Δ in equations (5.7) leads to the asymptotic solution

$$v_\infty = [\gamma_2^2 (1 + \Delta)^2 - u_2^2]^{-1/2} , \tag{5.8}$$

which, upon use of equation (5.7b), leads to

$$u_\infty \equiv u_2 v_\infty = \left(\frac{\sigma^2}{1 + 2\sigma} \right)^{1/2} , \tag{5.9a}$$

$$\beta_\infty = \frac{u_\infty}{\gamma_\infty} = \frac{\sigma}{1 + \sigma} . \tag{5.9b}$$

Kennel, Fujimura, and Okomoto (1983) found two characteristic solutions to the relativistic stellar wind problem at large distances from the wind source. The first should be identified with the upstream wind speed u_1; the second was given by equation (5.9a). Thus, a strong shock takes the flow speed from one characteristic wind solution to the other. Inclusion of finite u_2/u_1 effects would probably bring the asymptotic downstream flow speed to a value just above that given by equations (5.9).

Substituting the definitions (4.1) and (4.2), assuming $u_1 \approx \gamma_1$, and converting from normalized to true distance, we may show that

$$\frac{B^2}{8\pi} \xrightarrow[r \to \infty]{} \frac{L}{8\pi r^2 c} \left(\frac{1 + \sigma}{\sigma} + \frac{\sigma}{1 + \sigma} \right) \tag{5.10}$$

as z approaches infinity. Thus B is inversely proportional to r in the asymptotic limit. However, equation (5.10) indicates that, when σ is large, $B^2/8\pi \approx L/4\pi r^2 c$, whereas when σ is small, the magnetic pressure exceeds $L/4\pi r^2 c$ by a factor of $\frac{1}{2}\sigma$.

Equations (5.8)–(5.10) convey an important physical point. Magnetized stellar winds cannot expand to zero velocity but tend toward a constant asymptotic speed, because they must continue to transport magnetic flux outward in the absence of magnetic dissipation. No matter how weakly magnetized the wind upstream of the shock, the magnetic field will eventually control the dynamics of the postshock flow. This fact will have great significance for matching the postshock flow solution with that of the expanding supernova remnant. Nowhere can the flow β fall below $\sigma/1 + \sigma$, and since the remnant β is small, only small-σ solutions will satisfy the boundary conditions.

c) *Large-σ Limit*

Inserting the approximate expressions $u_2^2 \approx \sigma$ and $\Delta \approx \frac{1}{2}\sigma$ into equations (5.7), dropping δ, squaring, and keeping the leading terms in $1/\sigma$ reduces equations (5.7) to a quartic

$$w^4 - 2\eta w^3 + \eta = 0 \tag{5.11a}$$

(where $w = v^{2/3}$ and $y = z^{2/3}$), which may be solved using standard techniques. Its resolvent cubic is $y^3 - 4\eta y - 4\eta^3 = 0$, whose real solution is

$$y = \eta [(2 + 2f)^{1/3} + (2 - 2f)^{1/3}] , \tag{5.11b}$$

where

$$f = \left(1 - \frac{16}{27\eta^3} \right)^{1/2} . \tag{5.11c}$$

The solution to equation (5.11a) which satifies $v = 1$ at $z = 1$ is given by $2w = y + R - D$, where

$$R = (y + \eta^2)^{1/2}\,; \quad D = \left(2\eta^2 - y + \frac{2\eta^3}{R}\right)^{1/2}. \quad (5.11d)$$

We evaluated equations (5.11) numerically to obtain $v(z)$, whose behavior is so simple that it need not be plotted. The quantity v diminishes from 1 at $z = 1$ to $v = 0.76$ at $z = 5$, and it decreases more slowly thereafter. At $z = 30$, v is 0.722, very close to its asymptotic value of $1/\sqrt{2}$.

In summary, when σ is large, the four speed in the postshock flow decreases monotonically from $\sqrt{\sigma}$ to $\sqrt{(\sigma/2)}$, the flow remains relativistic, and the magnetic field strength is almost exactly proportional to $1/r$. This behavior is forced by the requirement that the flow carry a large toroidal magnetic flux outward.

d) Small-σ Limit

When $\sigma < 1$, the postshock flow speed will be nonrelativistic everywhere, and we may set γ and γ_2 approximately equal to unity. Then equations (5.7) reduce to a cubic

$$t^3 - \frac{\Delta}{1+\Delta}\,t^2 - \frac{z^2}{1+\Delta} = 0\,, \quad (5.12a)$$

$$t = (vz^2)^{1/3}\,, \quad (5.12b)$$

whose single real solution may again be obtained by standard techniques:

$$v = \frac{1}{2(1+\Delta)}\,\frac{G^3}{x^2}\,, \quad (5.12c)$$

$$G = 1 + \{1 + x^2 + [(1+x^2)^2 - 1]^{1/2}\}^{1/3} + \{1 + x^2 - [(1+x^2)^2 - 1]^{1/2}\}^{1/3}\,, \quad (5.12d)$$

$$x = \frac{z}{z_\Delta}\,, \quad z_\Delta = \left[\frac{2}{27}\,\frac{\Delta^3}{(1+\Delta)^2}\right]^{1/2}; \quad (5.12e)$$

when $x \ll 1$, G^3/x^2 approaches $27/x^2$, and when x is large, G^3/x^2 approaches 2.

Figures 3 and 4 were obtained by combining equation (4.11), which determines u_2 as a function of σ, with the solutions to equations (5.12), which yield the z dependence of u beyond the shock. The quantities at $z = 1$ in Figures 3 and 4 are the Rankine-Hugoniot solutions. The left-hand portion of Figure 3 surveys the dependence of the flow four speed $u(z)$ upon the magnetization parameter σ. When $\sigma = 1$, the flow speed $u(z)$ is weakly dependent on z, in qualitative agreement with the large-σ behaviour described by equations (5.11) above. In the opposite extreme case shown, $\sigma = 0.01$, $u(z)$, which is approximately $\frac{1}{3}$ just downstream of the shock, decreases first as $1/z^2$ before approaching its asymptotic value of $u_\infty \approx \sigma$. When $\sigma \leq 0.1$, the plasma pressure exceeds the magnetic pressure behind the shock, and the initial expansion is nearly hydrodynamical in nature. If the flow were hydrodynamic, the density and pressure would be approximately constant, and u would be proportional to $1/z^2$ downstream of the shock. Such quasi-hydrodynamic behavior persists until the magnetic pressure approaches equipartition, after which the flow approaches the constant velocity state characteristic of magnetically dominated flows.

The right-hand side of Figure 3 plots the magnetic field strength in the nebula, normalized to its strength in the wind upstream of the shock. When $\sigma = 1$, the shock frame field behind the shock is only slightly larger than that upstream, and decreases as $1/z$ thereafter. When $\sigma = 0.01$, the magnetic field is amplified by a factor 3 across the shock, *increases* even more downstream—roughly as z—eventually reaches a maximum at a characteristic normalized distance $\bar{z}$, to be estimated below, and only then approaches its final $1/z$ dependence. The quantity $\bar{z}$ may be located by equating the $x \ll 1$ and $x \gg 1$ approximations to equations (5.12c)–(5.12e), whereupon

$$\bar{z} = \left[\frac{\Delta^3}{(1+\Delta)^2}\right]^{1/2} \approx (3\sigma)^{-1/2}\,, \quad (5.13)$$

where we substituted the small-σ approximation, $\Delta \sim \frac{1}{3}\sigma \gg 1$, to arrive at the second expression on the right-hand side of equation (5.13).

By expanding equations (5.12c)–(5.12e), it is easy to show that $v(z)$ is approximately

$$v(z) \approx \frac{1}{1+\Delta}\left[1 + \left(\frac{\bar{z}}{z}\right)^{2/3}\right] \quad (5.14)$$

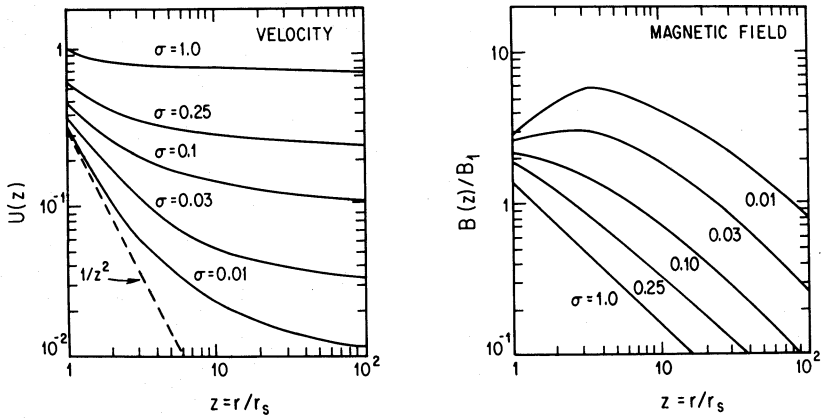

FIG. 3.—*Postshock speed and magnetic field.* The left-hand graph plots the four velocity, and the right-hand graph, the magnetic field normalized to its upstream strength, against $z = r/r_S$, for values of σ in the range 10^{-2} to 1. The values at $z = 1$ emerge from solutions of the Rankine-Hugoniot relations. High-σ flows have u nearly constant and the magnetic field nearly proportional to $1/r$. Low-σ flows have a quasi-hydrodynamic region within $\bar{z} \lesssim (3\sigma)^{-1/2}$; beyond $\bar{z}$, the spatial dependencies of u and B/B_1 resemble those of the highly magnetized large σ-flows.

when $z \gg \bar{z}$. If σ is small, $u_2 \approx \frac{1}{3}$, $\Delta \approx \frac{1}{3}\sigma$, and $\bar{z} \sim (3\sigma)^{-1/2}$, so that when z exceeds $\bar{z}$,

$$u(z) \equiv u_2 v(z) \approx \sigma[1 + (3\sigma z^2)^{-1/3}] . \quad (5.15)$$

In § IV, we will use the approximate solution (5.15) to illustrate our discussion of how the boundary conditions imposed by the supernova remnant may be used to estimate the shock radius.

Figure 4 plots the temperature, normalized to the upstream flow energy per particle, $u_1 mc^2$, for σ in the range 0.01–1. For large σ, the shock heating is relatively small, and the temperature decreases monotonically beyond the shock. When σ is small, the downstream temperature nearly equals the upstream flow energy per particle, remains constant throughout the hydrodynamic region, $z < \bar{z}$, and only begins to decline after $z = \bar{z}$.

VI. CONFINEMENT OF THE PULSAR WIND

a) *Introductory Remarks*

Having described the family of steady nebular flow solutions in the previous section, we now turn to the more subtle task of deciding whether any of its members is consistent with the boundary conditions imposed by the surrounding remnant, and if so, which one. In inquiring where to place the boundary, what the boundary conditions should be, and what observations can tell us about them, we confront our simple assumptions with complex reality.

The questions about the location of the boundary and the form of the boundary conditions are intimately related. If, as Rees and Gunn (1974) did, and we shall do, one idealizes the present boundary as a thin conducting layer, it seems natural to place it at the outermost radio contour. Observations of synchrotron radiation tell us where the magnetized flow goes, and we expect the remnant to have a minuscule primordial field, so the last radio contour should indicate where the flow terminates. At 2.7 GHz, the radio emissions appear to fill a prolate spheroid with semiminor and semimajor axes of 1.5 and 2.1 pc, respectively (Wilson 1972). The outer boundaries of the deep optical nebula (van den Bergh 1970) and of the filamentary network (Wyckoff *et al.* 1976; Clark *et al.* 1983) coincide with the radio boundary. On this basis, it seems reasonable to place the wind-remnant interface at the radius $r_N \approx 1.8$–2 pc in a spherical model. On the other hand, our neglect of the time dependence of the flow, and its interaction with the filaments, becomes progressively more dubious with increasing distance from the pulsar, so our flow solution may be accurate only part of the way to r_N, a possibility that can be tested by comparing the theoretical properties of the flow at r_N with observation.

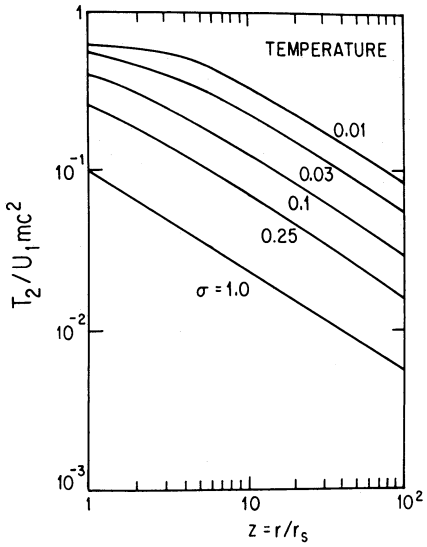

FIG. 4.—*Postshock temperature.* This figure plots the temperature normalized to the upstream flow energy per particle, $u_1 mc^2$, against z. Low-σ flows are hotter than high-σ flows, and the temperature remains nearly constant in the quasi-hydrodynamic region, $z < \bar{z}$.

If the wind-remnant interface is comoving with the flow, the sum of the nebular plasma, magnetic, and electric pressures will equal, or slightly exceed, the remnant's plasma pressure, P_R, at the interface. The secondary boundary condition, that the wind speed match that of the remnant at the moving interface, restricts the range of σ for which steady state solutions exist. Recall that the wind three speed, β, always exceeds $\sigma/1 + \sigma$, so that σ must be small, since the remnant's expansion speed is nonrelativistic. Therefore, although we surveyed the properties of flows with both large and small σ in §§ IV and V, we will concentrate on flows with $\sigma \leq 10^{-2}$ in the discussion to follow.

b) *Estimates of the Flow Speed near the Wind-Remnant Interface*

Several independent arguments suggest that V_R is about 2000 km s^{-1}. First of all, the average radius of the nebula, r_N, which is 1.8–2 pc, is consistent with an average expansion speed of about 2000 km s^{-1}. Second, we can estimate the flow speed in the remnant near r_N in two partially independent ways. In constructing Figure 1, we implicitly argued, on the basis of Murdin and Clark's Hα observations, that 5 pc is a reasonable estimate for the average distance from the pulsar to the outer edge of the supernova remnant in a spherical model. This distance corresponds to an average expansion speed of 5000 km s^{-1}, which, if mass pickup has indeed been negligible, is still close to the present expansion speed. If the remnant's expansion was homologous, as is often assumed for young remnants (e.g., Gull 1973, 1975), the flow speed at r_N would be $\frac{2}{5}$ of that at the leading edge, or about 2000 km s^{-1}. Clearly this estimate is rough, because of the spheroidal rather than spherical shape of both nebula and remnant, but it again suggests that V_R of order 2000 km s^{-1} is reasonable. Finally, we may obtain a lower limit on the wind speed in the nebula from the observed motions of the filaments, which are consistent with initial expansion speeds of 1700 km s^{-1} and 1100 km s^{-1} along the major and minor axes of the nebula, respectively (Trimble 1971). This leads to an average expansion speed of about 1400 km s^{-1}. The filament's speeds increase approximately linearly with distance from the pulsar, albeit with striking exceptions (Trimble 1968). The fastest filaments in the nebula, which are nearest its outer edge, have speeds of about 1800 km s^{-1} (Trimble 1968; Wyckoff and Murray 1977; Clark *et al.* 1983).

Because the nebular magnetic field is observed to be wrapped around the filaments (Wilson 1972; Swinbank 1980), MHD reasoning suggests that the pulsar wind flows around the filaments and penetrates to the massive remnant, consistent with the fact that the outer boundaries of the synchrotron radiation and filamentary shell coincide. This also suggests that the observed filament speeds bound the local wind speed from below.

c) Observational Constraints on the Confining Pressure

The less direct estimates of the pressure near the nebula-remnant interface are more uncertain than those of the flow speed. The average pressure in the nebula can be bounded from below from observations of synchrotron radio emissions. A physically meaningful upper bound on the pressure at the inner edge of the halo can be derived from Schattenburg *et al.*'s (1980) limits on X-ray line intensities.

A lower limit on a volume average of the pressure can be obtained from the minimum energy density in the magnetic field and relativistic electrons and positrons required to produce the nebular synchrotron emission. This estimate depends on the maximum frequency ν_{max} to which the $\nu^{-0.26}$ radio spectrum extends before steepening. We have carried out the minimum energy density computation therefore for $\nu_{max} = 10^{11}$ Hz, to which the characteristic radio spectrum certainly extends, and for $\nu_{max} = 10^{14}$ Hz, at which frequency the spectrum is certainly breaking. The range $\nu_{max} = 10^{11}$–10^{14} Hz spans the frequencies where measurements are sparsest. Assuming the nebula is a prolate spheroid with major and minor axes of 2.1 and 1.5 pc, respectively, the nebular volume is 5.34×10^{56} cm^{-3}. For this volume, we find that the average magnetic plus relativistic particle pressure, magnetic field, and total energy are, 3.6×10^{-9} dyn cm^{-2}, 2.5×10^{-4} G, and 3.2×10^{48} ergs, and 10×10^{-9} dyn cm^{-2}, 4.2×10^{-4} G, and 8.7×10^{48} ergs for $\nu_{max} = 10^{11}$ and 10^{14} Hz, respectively. These estimates are generally consistent with others in the literature.

The precise relationship between pressure limits derived from volume-averaged radio observations and the pressure at the outer boundary of the nebula is unclear, especially for a configuration such as ours, in which the ratio of magnetic to plasma pressure varies continuously throughout the flow. Figure 5 plots the ratio of magnetic to total pressure against z for $\sigma = 0.01$, 0.003, and 0.001 calculated using equations (5.12a)–(5.12e) and (6.1). Equipartition is reached where $z = \bar{z}$, and $\bar{z}$ is defined in equation (5.13). All things being equal, one expects the pressure at the nebula-remnant interface to be somewhat less than its volume average.

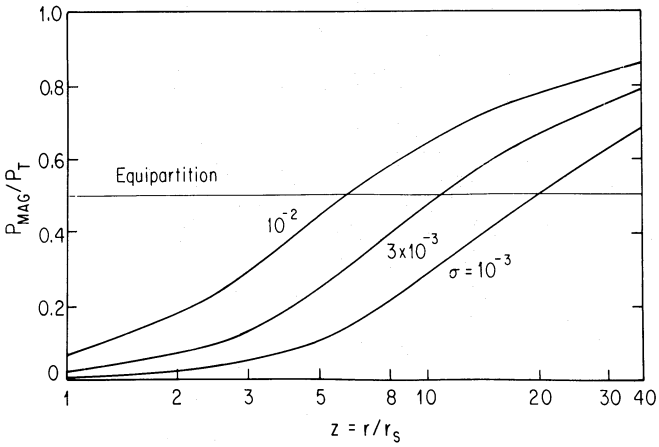

FIG. 5.—*Ratio of magnetic to total pressure.* The ratio of the magnetic pressure, P_{MAG}, to the total pressure, P_T (eq. [6.1]), is plotted as a function of $z = r/r_S$ for $\sigma = 0.01$, 0.003, and 0.001. This ratio is independent of the luminosity of the pulsar and the radius of the shock. Equipartition is momentarily achieved at the points $z \approx \bar{z}$, indicated by the intersections of the line marked "equipartition" with the calculated curves. When $z < \bar{z}$, the plasma pressure dominates the magnetic, and vice versa when $z > \bar{z}$.

Spectral observations of the filaments give another, ambiguous, estimate of the pressure in the nebula. Multiplying the densities and temperatures determined by Fesen and Kirshner (1982) leads to filament pressures in the range $1–10 \times 10^{-9}$ dyn cm^{-2}, with the majority in the range $1–3 \times 10^{-9}$ dyn cm^{-2}. While these estimates are consistent with the pressure bound derived from the radio spectrum, it is not known whether the filaments are in pressure equilibrium with the surrounding flow.

An upper limit on the pressure in the confining remnant may be estimated from the failure to detect X-ray line emission from thermal plasma using the *Einstein* focal plane crystal spectrometer (Schattenburg *et al.* 1980). Earlier searches at lower sensitivity had also been carried out by Kestenbaum *et al.* (1977), Parsignault *et al.* (1978), and Pravdo and Serlemitsos (1981). Schattenburg *et al.* (1980) took three $3' \times 30'$ aperture, east-west–oriented strips, and two $6'$ diameter circular exposures; two strips, their positions 1 (north) and 3 (south), which excluded the synchrotron X-ray source, provided the most stringent upper limits on the X-ray line flux from the remnant. For position 3, the Fe XVII ($E = 0.826$ keV) and O VIII ($E = 0.654$ keV) upper limit line fluxes were 6×10^{-12} and 6.3×10^{-12} ergs cm^{-2} s^{-1}, respectively. By modeling the putative thermal plasma region as a spherical shell of radius $210'' = 2.1$ pc and thickness $\Delta R/R = 0.1$, Schattenburg *et al.* (1980) ruled out a thermal X-ray source as intense as that reported by Toor, Palmieri, and Seward (1976) and suggested that Toor *et al.* had observed synchrotron X-rays that had been scattered by interstellar grains.

For the same spherical shell model, the upper limit line fluxes bound the thermal plasma density and pressure. From the tables of Raymond and Smith (1977), the upper bound emission measures $n_e^2 V$ for slot position 3 are 6×10^{56} cm^{-3} and $2.2–4.6 \times 10^{57}$ cm^{-3} for Fe XVII and O VIII, respectively, assuming $T_e \approx 0.6–1.0 \times 10^7$ K. The position 3 slit intercepted a volume $V \approx 10^{56}$ cm^3, approximately 30% of the $7'$ diameter spherical shell. The thermal electron density within the shell is thus bounded by $n_e \approx 3–6$ cm^{-3}, and the total thermal plasma pressure is limited by $5–10 \times 10^{-9}$ dyn cm^{-2}. These estimates may err somewhat because of Raymond and Smith's (1977) assumptions of steady state ionization and excitation.

The upper limit on the remnant pressure appears consistent with the synchrotron lower bound derived above, given the limited accuracy of either estimate. Trimble and Rees (1970) derived an upper bound to the average nebular pressure, by assuming that the pulsar accelerates $0.8\ M_\odot$ of filamentary material at a rate no more than 3 times the average historical rate, 1.4×10^{-3} cm s^{-2}. The limit on the remnant pressure above appears to rule out a present acceleration of the filaments greater than about 10% of the average historical rate. The limit still permits a moderately strong shock-heated X-ray source in the remnant, whose properties we speculate about in Appendix A.

In summary, it appears the flow speed is about 2000 km s^{-1}, and the pressure is in the range $1–10 \times 10^{-9}$ dyn cm^{-2} near the nebula-remnant interface.

d) Are the Boundary Conditions Satisfiable?

We will approach the above question in two ways. First, we will assume that the locations r_S and r_N of the reverse shock and nebula boundary are fixed by observation and then compare the predicted speed and pressure at r_N with observation. Second, we will assume that the remnant speed and press-

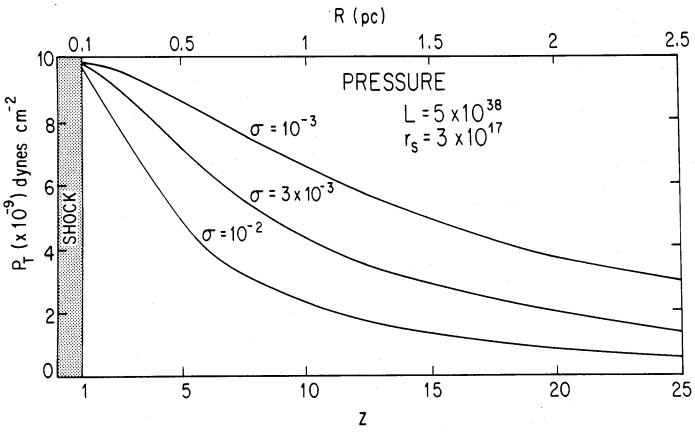

FIG. 6.—*Dependence of nebular pressure on radial distance.* The total pressure is plotted as a function of z (*bottom scale*) and radial distance (assuming $r_S = 0.1$ pc and $d = 2$ kpc, *top scale*), for $\sigma = 0.01$, 0.003, and 0.001. We assumed the pulsar luminosity was 5×10^{38} ergs s^{-1}. The pressure difference between the inner and outer nebula is about 10×10^{-9} dyn cm^{-2} in all three cases, and the pressure diminishes more slowly the smaller the value of σ.

ure at r_N are known and compare the calculated r_S with the position of the reverse shock inferred from the termination of the underluminous zone. Both methods link independent measurements by theory.

The total pressure P_T in the postshock flow is

$$P_T = P + \frac{E^2 + B^2}{8\pi} = \frac{L}{4\pi r_S^2 c(1+\sigma)} \times \left[\frac{P_2}{n_1 mc^2 u_1^2}(vz^2)^{-4/3} + \frac{\sigma}{z^2}\left(1 + \frac{1}{2u_2^2 v^2}\right)\right], \quad (6.1)$$

where $P_2/n_1 mc^2 u_1^2$ and u_2 are determined by the Rankine-Hugoniot relations, and v is given by equations (5.12a)–(5.12e). Figure 6 plots the dependence of the total pressure against radial distance from the pulsar, assuming the pulsar luminosity $L = 5 \times 10^{38}$ ergs s^{-1} and $r_S \approx 3 \times 10^{17}$ cm (10″), for $\sigma = 10^{-3}$, 3×10^{-3}, and 10^{-2}. The value of P_T scales as I/d^2, where I is the pulsar moment of inertia, and d is the distance to the Crab nebula. The pressure is approximately $\frac{2}{3}(L/4\pi r_S^2 c)$ behind the shock and diminishes monotonically with distance; the total pressure difference between the inner and outer nebula is about 10×10^{-9} dyn cm^{-2}. Figure 7 plots the magnetic field as a function of radial distance for the same parameters as Figure 6.

Figure 8 plots the dependences of P_T and the flow speed upon σ at radial distances of 1, 2, and 3 pc from the pulsar. We emphasize, with heavy lines, the solutions for $r = 2$ pc—a reasonable estimate for the radius of the nebula in a spherical model. The closest agreement between the predicted and observed flow speeds occurs for $\sigma = 0.003$; the calculated pressure for $\sigma = 0.003$ at $r = 2$ pc is in the low end of the range of pressures estimated from observation.

Given the remnant pressure, P_R, its flow speed, V_R, at r_N, and a value of σ, we could locate the reverse shock by specifying a flow solution at r_N and following it inward until the Rankine-Hugoniot jump conditions with the upstream wind were satisfied. We will illustrate this procedure by using the $z \gg \bar{z}$ limits

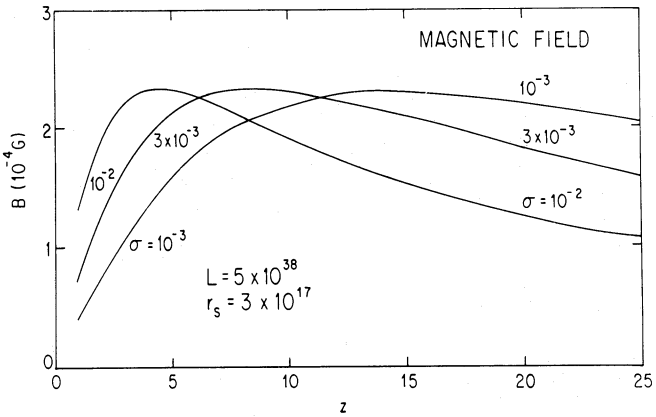

FIG. 7.—*Dependence of magnetic field on radial distance.* The magnetic field is plotted as a function of z for the same parameters as in Fig. 6. The magnetic field rises to a maximum of 2.3×10^{-4} G in all three cases, and the smaller the value of σ, the larger it is in the outer nebula. Since the magnetic field has the same maximum value, radio observations without adequate spatial resolution cannot distinguish between the values of σ. If σ should be so small that $\bar{z} = z_N$, the field will maximize at the boundary of the nebula. Decreasing σ further will then reduce the nebular field, which will approach 0 as $\sigma \to 0$.

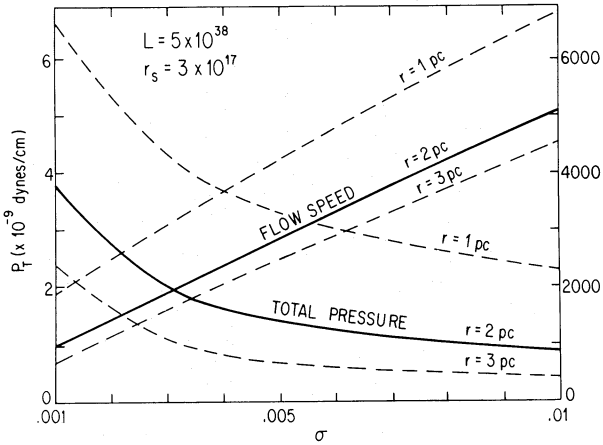

FIG. 8.—*Total pressure and flow speed at r = 1, 2, and 3 parsecs.* This figure helps us to gauge the extent to which the flow boundary conditions are satisfiable. The total pressure (*left-hand scale*) and flow speed (*right-hand scale*) are plotted as functions of σ for $r = 1$, 2, and 3 pc, assuming $L = 5 \times 10^{38}$ ergs s^{-1} and $r_S = 3 \times 10^{17}$ cm. The observed boundary of the nebula is near $r = 2$ pc, so we have emphasized this case by heavy lines. For $\sigma \approx 0.003$, the flow speed is 2000 km s^{-1}, consistent with observational estimates, and the pressure is 2×10^{-9} dyn cm^{-2}, at the low end of the observational range.

of the small-σ solutions obtained in § V. The velocity boundary condition becomes

$$\beta_R \approx \frac{V_R}{c} \approx (1 + \lambda)\sigma \,, \tag{6.2a}$$

$$\lambda \equiv (3\sigma z_N^2)^{-1/3} \,, \tag{6.2b}$$

where $z_N = r_N/r_S$. We then take the $\sigma \ll 1$ limit of equation (6.1) and expand all terms involving z to first order in λ, which for the best fit parameters that we shall obtain will not be very small; however, the relations obtained to first order in λ reveal the physical scalings we wish to delineate:

$$P_R \approx \frac{L}{8\pi r_N^2 \sigma c}\left(1 - \frac{14\lambda}{9}\right). \tag{6.3}$$

Equations (6.2) and (6.3) may be rewritten in forms that render the calculation of r_S explicit:

$$\frac{r_S}{r_N} \approx \sqrt{\sigma}\left(3^{1/3}\,\frac{\beta_R - \sigma}{\sigma}\right)^{3/2} , \tag{6.4a}$$

$$\frac{r_S}{r_N} \approx \sqrt{\sigma}\left(1 - \frac{8\pi r_N^2 P_R \sigma c}{L}\right), \tag{6.4b}$$

where numerical factors of order unity have been suppressed for clarity. Equations (6.4) imply that solutions exist only for $\beta_R > \sigma$ and $P_R < L/3\pi r_N^2 V_R$, where $V_R \approx \sigma c$ is the remnant speed at the interface. If P_R exceeds the value estimated above, the reverse shock would be driven back to the pulsar.

If, as we have argued, the quantities in parentheses in equation (6.4) are of order unity, then $r_S/r_N \approx \sqrt{\sigma}$, which is 1/18 for $\sigma = 0.003$, in rough accord with observation. The scaling $r_S/r_N \approx \sqrt{\sigma} \approx \beta_R$ is also the one Rees and Gunn (1974) arrived at by assuming that the reservoir of energy of pulsar origin accumulated steadily over the lifetime of the nebula.

In summary, if $\sigma = 0.003$, both the flow and pressure boundary conditions at the nebula-remnant interface appear to be satisfiable, and the reverse shock will stand approximately where it is inferred to be. The fact that the calculated pressure is at the low end of the range of estimated pressures suggests that while effects neglected here, such as time dependence and flow-filament interactions, may eventually need to be included, the present model gives a reasonable first accounting of the dynamics of the Crab nebula. The flow speed and pressure in the outer nebula do appear to be reconcilable in a simple magnetohydrodynamic model whose parameters are adjustable within a narrow range.

VII. DISCUSSION

This paper is the second in a series of three. In the first, Kennel, Fujimura, and Okamoto (1983) reanalyzed the classical problem of a relativistic stellar wind in magnetic monopole geometry (Michel 1969), including the effects of finite source temperature. This work clarified the difference between cold, centrifugally driven winds—the only ones considered seriously thus far in the literature—and hot, thermally driven winds. Only winds that are relativistically hot at the source can achieve relativistically large fast Mach numbers, and only such winds can have the strong standing reverse shock integral to Rees and Gunn's (1974) and our models. The present paper is a self-consistent magnetohydrodynamic reexamination of Rees and Gunn's spherically symmetric model of the Crab nebula that introduces into it greater conceptual specificity and applies to it more modern and different observational information. Our analysis illuminates the central role played by the ratio, σ, of the magnetic to plasma luminosity of the pulsar wind. The confinement boundary conditions imposed upon the pulsar wind are best satisfied if σ is about 3×10^{-3}. For this value of σ, the pressure and flow speed in the outer nebula appear to be consistent with the position of the reverse shock in the pulsar wind inferred from radio, optical, and X-ray synchrotron continuum observations. This steady MHD model can be tested by the extent to which it accounts for observations not used to specify the model. In the third paper of this series (Kennel and Coroniti 1984), we will compute the spectrum and spatial distribution of the synchrotron radiation from the Crab nebula, using the flow solutions developed here. Although we will defer a detailed critique until after theory is confronted by observation in that paper, we note here that a low-σ positronic flow has desirable features that can help explain how the Crab pulsar converts its spin-down luminosity into synchrotron luminosity with such high efficiency. Both ions and electrons radiate in a positronic flow. Much more flow energy is converted into random particle energy behind low-σ shocks. Moreover, the magnetic field builds up downstream of low-σ shocks, a fact which may help explain the small size of the hard X-ray emitting region surrounding the pulsar.

The status of our implied conclusion, that the Crab pulsar converts more than 99% of its spin-down power into flowing relativistic particles before the flow crosses 10% of the nebula, depends upon the realism of the assumptions used to reach it. For example, our toroidal magnetic field approximation eliminated 2 degrees of freedom (associated with the rotational discontinuity and slow shock) that increase the flexibility of the flow to satisfy its boundary conditions. We do expect these discontinuities to propagate slowly and therefore not to affect the overall pressure balance in the nebula significantly. More importantly, we assumed a steady state. By reducing the richness of the full magnetohydrodynamic equations, we limited the range of possible solutions. As a result, only one value of σ could satisfy the boundary conditions.

We must emphasize that our solution requires σ to be small only downstream of the shock. The conclusion that the flow has a small σ when it leaves the pulsar's light cylinder is not necessarily warranted. Furthermore, the monopole wind model underlying our simplified nebular flow model neglects the small-scale sector structure impressed on the flow by a misaligned dipole field. A further investigation is required to see if this situation mimics or leads to a low-σ quasi–steady state flow downstream of the shock.

One can ask, what happens to an inherently high-σ flow that is confined by a slowly moving remnant? This paper suggests that either the interactions with the filaments neglected here do decelerate the flow, or the flow is fundamentally unsteady, or both. Kundt and Krotschek (1980) and Kundt (1981) also noted the dilemma we associated here with high-σ flows: the pressure at the edge of the nebula would be too small. They therefore argued that the pressure is largely provided by pulsar waves that reflect many times from the boundary of the nebula. Should pulsar waves be absent, it appears likely that, when σ is large, a large head of pressure would build up near the nebula-remnant interface; this piston would then drive an unsteady flow in the nebula. Rees and Gunn (1974) divided the pulsar luminosity into wind and wave components but left the wave luminosity a free parameter that could help satisfy the pressure boundary condition, if need be. If our analysis is correct, a

significant wave luminosity is not absolutely necessary to balance the confining pressure.

Further observations will certainly clarify theories of the Crab nebula. The uncertainties in our model become progressively greater with increasing distance from the pulsar. The time for the flow to pass from the pulsar to the edge of the nebula turns out to be the age of the system. The plasma and magnetic field in the distant nebula were injected long ago and may have been subject to events—such as the one suggested by Chevalier (1977) in which a core shell accelerated by the pulsar collided with the supernova envelope—that do not occur, and are not observable, today. We have only the most idealized picture of the present nebula-remnant interface, nor do we know whether filaments are forming today. Thus high-resolution studies of the interaction of the nebular flow with the filaments and interface will be most valuable. Detection of thermal X-rays from the inner remnant would reveal the energetics of the nebula-remnant interaction, and the size of the X-ray region would indicate when it began. Studies of other plerionic remnants might be helpful, for such thermal X-rays might be relatively more prominent when the synchrotron X-ray emission from the pulsar wind has declined. In the meantime, the present evidence poses an interesting question for pulsar theory. Can the Crab pulsar convert so much of its power into flowing plasma, and if so, how?

We are pleased to acknowledge helpful discussions with R. Blandford, A. Cheng, F. S. Fujimura, C. McKee, F. C. Michel, V. Trimble, and especially J. Arons. The first draft of this paper was written at the Institute for Theoretical Physics, Santa Barbara, for whose hospitality we are grateful. This work was supported by NASA NSG-7341.

APPENDIX A

INTERNAL SHOCK CALCULATION

In this Appendix, we speculate about the properties of the shock that could have been created in the remnant by the pulsar interaction and that would be consistent with the upper limit remnant pressure derived in § VI*c*.

According to McKee (1974), the temperature T behind a strong hydrodynamic shock is given by $T = 1.2V_8^2$ keV, where V_8 is the shock speed in units of 1000 km s^{-1}. For $T = \frac{1}{2}$ (500 eV), $V = 650$ km s^{-1}. Such a shock could have moved no more than 0.6 pc from the nebula-remnant interface, the distance it would travel in 1000 yr. The soft X-ray luminosity L_x behind the shock would be $L_x = 5 \times 10^{-24}\langle n_e^2\rangle T^{1/2}\phi V$, where $\langle n_e^2\rangle$ is the mean-square electron density in the emitting volume V; ϕ, which depends upon the composition of the gas, should be about 2.5 for the hydrogenic stellar envelope. The mass M_x contained in the emitting volume is $M_x = \langle n_e\rangle\langle A/Z\rangle M_p V$, where $M_p = 1.6 \times 10^{-24}$ grams, the proton mass, and $\langle A/Z\rangle$ is the mass-to-charge ratio of the emitting ions. If ΔR is the thickness of the X-ray emitting shell, then $V = 4\pi R^2\Delta R$. We will assume that $\langle n_e\rangle \approx \langle n_e^2\rangle^{1/2}$, and that the emitting gas is fully ionized so that $\langle A/Z\rangle \approx 1$. Finally, we will scale the X-ray luminosity L_x to 10^{35} ergs s^{-1} by writing $L_x \approx 10^{35} l$ ergs s^{-1}. If we choose the representative values $R \approx r_N \approx 2$ pc, $T = \frac{1}{2}$, $\Delta R \approx 0.3$ pc, and define $\phi' = \phi/2.5$, we find that $V \approx 4 \times 10^{56}$ cm^{-3}, and that

$$\langle n_e\rangle \approx 5(l/\phi')^{1/2}\ \text{cm}^{-3}\ ; \qquad M_x \approx 1.5(l/\phi')^{1/2}\ M_\odot\ ; \tag{A1}$$

$\langle n_e\rangle$ and M_x are proportional to $(\Delta R)^{-1/2}$ and $(\Delta R)^{+1/2}$, respectively. The total energy E of the shocked gas is approximately

$$E \approx 2(\tfrac{5}{2}\langle n_e\rangle T) \approx 10^{49}(l/\phi')^{1/2}\ \text{ergs}\ . \tag{A2}$$

While the X-ray luminosity reported by Toor, Palmieri, and Seward (1976), $l = 40$, is probably too large to have been produced by the pulsar interaction, the energy required to produce a shock that radiates 10^{35} ergs s^{-1} in thermal X-rays behind it is smaller than, but comparable to, the total energy radiated by the pulsar over its lifetime. Moreover, its postshock electron density would be consistent not only with the upper limit derived in § VI*c*, but also with that expected behind a strong shock propagating into the envelope, whose mean density Murdin and Clark (1981) estimated to be about 1 cm^{-3}.

REFERENCES

Ardavan, H. 1976, *Ap. J.*, **206**, 822.
———. 1979, *M.N.R.A.S.*, **189**, 397.
———. 1981, *Ap. J.*, **251**, 674.
Arnett, W. P. 1975, *Ap. J.*, **195**, 727.
Arons, J. 1972, *Ap. J.*, **177**, 395.
———. 1979, *Space Sci. Rev.*, **24**, 437.
———. 1981*a*, in *IAU Symposium 95, Pulsars*, ed. W. Sieber and P. Wielebinski (Dordrecht: Reidel), p. 69.
———. 1981*b*, *Ap. J.*, **248**, 1099.
———. 1983, private communication.
Arons, J., and Scharlemann, E. T. 1979, *Ap. J.*, **231**, 854.
Aschenbach, N., and Brinkmann, W. 1975, *Astr. Ap.*, **41**, 147.
Asseo, E., Kennel, C. F., and Pellat, R. 1978, *Astr. Ap.*, **65**, 401.
Barnard, J. J., and Arons, J. 1982, *Ap. J.*, **254**, 713.
Blandford, R. D. 1972, *Astr. Ap.*, **20**, 135.
Blandford, R. D., Kennel, C. F., McKee, C. F., and Ostriker, J. P. 1983, *Nature*, **301**, 586.
Charles, P. A., and Culhane, J. L. 1977, *Ap. J.* (*Letters*), **211**, L23.
Cheng, A., and Ruderman, M. S. 1977, *Ap. J.*, **216**, 365.
Cheng, A., Ruderman, M. A., and Sutherland, P. G. 1976, *Ap. J.*, **203**, 208.
Chevalier, R. A. 1976, *Ap. J.*, **207**, 872.
Chevalier, R. A. 1977, in *Supernovae*, ed. D. N. Schramm (Dordrecht: Reidel), p. 53.
Clark, D. H., Murdin, P., Wood, R., Gilmozzi, R., Danziger, J., and Furr, A. W. 1983, *M.N.R.A.S.*, **204**, 415.
Davidson, K. 1979, *Ap. J.*, **228**, 179.
Davidson, K., *et al.* 1982, *Ap. J.*, **253**, 696.
Davison, P. J. N., Culhane, J. L., and Morrison, L. V. 1975, *Nature*, **253**, 610.
Dennefeld, M. 1983, in *IAU Symposium 101, Supernova Remnants and Their X-ray Emission*, ed. P. Gorenstein and I. J. Danzinger (Dordrecht: Reidel).
Fawley, W. M., Arons, J., and Scharlemann, E. T. 1977, *Ap. J.*, **217**, 227.
Fesen, R. A., and Kirshner, R. P. 1982, *Ap. J.*, **258**, 1.
Fukada, Y., *et al.* 1975, *Nature*, **255**, 465.
Goldreich, P., and Julian, W. H. 1969, *Ap. J.*, **157**, 869.
———. 1970, *Ap. J.*, **160**, 971.
Gorenstein, P., Harnden, F. R., Jr., Mitchell, M., and Seward, F. D. 1982, *Bull. AAS*, **159**, 865.
Gull, S. F. 1973, *M.N.R.A.S.*, **161**, 47.
———. 1975, *M.N.R.A.S.*, **171**, 263.
Gull, T. R., and Fesen, R. A. 1982, *Ap. J.* (*Letters*), **260**, L75.
Gunn, J. E., and Ostriker, J. P. 1971, *Ap. J.*, **165**, 523.
Hartmann, L., and MacGregor, K. B. 1980, *Ap. J.*, **242**, 260.

Henry, R. B. C., and MacAlpine, G. M. 1982, *Ap. J.*, **258**, 11.
Hillebrandt, W. 1982, *Astr. Ap.*, **110**, L3.
Hogg, D. E., MacDonald, G. H., Conway, R. G., and Wade, C. M. 1969, *A.J.*, **74**, 1206.
Holloway, N. 1973, *Nature*, **246**, 13.
Holzer, T. E. 1972, *J. Geophys. Res.*, **77**, 5407.
Kennel, C. F., and Coroniti, F. V. 1984, *Ap. J.*, **283**, 710.
Kennel, C. F., Fujimura, F. S., and Okamoto, I. 1983, *J. Ap. Geophys. Fluid Dyn.*, **26**, 147.
Kennel, C. F., Fujimura, F. S., and Pellat, R. 1979, *Space Sci. Rev.*, **24**, 407.
Kennel, C. F., and Pellat, R. 1976, *J. Plasma Phys.*, **15**, 335.
Kennel, C. F., Schmidt, G., and Wilcox, T. 1973, *Phys. Rev. Letters*, **31**, 1364.
Kestenbaum, H. L., Ku, W., Novick, R., and Wolff, R. 1975, *Ap. J.* (*Letters*), **202**, L15.
———. 1976, *Ap. J.* (*Letters*), **203**, L57.
Kestenbaum, H. L., Wolff, R. S., Long, K. S., Novick, R., and Weiskopf, M. C. 1977, *Ap. J.* (*Letters*), **216**, L27.
Ku, W. H., Kestenbaum, H. L., Novick, R., and Wolff, R. S. 1976, *Ap. J.*, **204**, 177.
Kundt, W. 1981, in *IAU Symposium 95*, *Pulsars*, ed. W. Sieber and P. Wielebinski (Dordrecht: Reidel).
Kundt, W., and Krotschek, E. 1980, *Astr. Ap.*, **83**, 1.
Landstreet, J. D., and Angel, J. R. P. 1971, *Nature*, **230**, 103.
Leboeuf, J. N., Ashour-Abdalla, M., Tajima, T., Kennel, C. F., Coroniti, F. V., and Dawson, J. M. 1982, *Phys. Rev. A*, **25**, 1023.
Makishima, K., Ogawara, Y., Matsuoka, M., Oda, M., Miyamoto, S., Pelling, R. M., Peterson, L. E., and Paciesas, W. S. 1981, *Space Sci. Rev.*, **30**, 259.
Matveenko, L. I. 1972, *Soviet Astr.—AJ*, **15**, 918.
Matveenko, L. I., and Kostenko, V. I. 1979, *Australian J. Phys.*, **32**, 105.
Matveenko, L. I., and Meeks, M. L. 1973, *Soviet Astr.—AJ*, **16**, 790.
Max, C. 1973, *Phys. Fluids*, **16**, 1277.
Max, C., and Perkins, F. 1971, *Phys., Rev. Letters*, **27**, 1342.
———. 1972, *Phys., Rev. Letters*, **29**, 1731.
McKee, C. F. 1974, *Ap. J.*, **188**, 335.
Michel, F. C. 1969, *Ap. J.*, **157**, 1183.
———. 1973*a*, *Ap. J.*, **180**, 207.
———. 1973*b*, *Ap. J.* (*Letters*), **180**, L133.
———. 1974, *Ap. J.*, **187**, 585.
Minkowski, R. 1971, in *IAU Symposium 46*, *The Crab Nebula*, ed. R. Davies and F. Smith (Dordrecht: Reidel), p. 241.
Murdin, P., Clark, D. H. 1981, *Nature*, **294**, 543.
Nomoto, K., Spaeks, W. M., Fesen, R. A., Gull, T. R., Miyaji, S., and Sugimoto, D. 1982, *Nature*, **299**, 803.
Okamoto, I. 1978, *M.N.R.A.S.*, **185**, 69.
Palmieri, J. M., Seward, F. D., Toor, A., and Van Flandern, T. C. 1975, *Ap. J.*, **202**, 494.
Parsignault, D. R., Delvaille, J. P., Epstein, A., Grindlay, J. E., and Schnopper, H. W. 1978, *Ap. J.*, **226**, 486.
Piddington, J. H. 1957, *Australian J. Phys.*, **10**, 530.
Pravdo, S. H., and Serlemitsos, P. 1981, *Ap. J.*, **246**, 484.
Raymond, J. C., and Smith, B. W. 1977, *Ap. J. Suppl.*, **35**, 419.
Rees, M. J. 1971*a*, in *IAU Symposium 46*, *The Crab Nebula*, ed. R. D. Davies and F. G. Smith (Dordrecht: Reidel), p. 407.
———. 1971*b*, *Nature Phys. Sci.*, **230**, 55.
Rees, M. J., and Gunn, J. E. 1974, *M.N.R.A.S.*, **167**, 1.
Ricker, G. R., Scheepmaker, A., Ryckman, S. G., Bellintine, J. E., Doty, J. P., Downey, P. M., and Lewin, W. H. G. 1975, *Ap. J.* (*Letters*), **197**, L83.
Ruderman, M. A. 1972, *Ann. Rev. Astr. Ap.*, **10**, 427.
Ruderman, M. A., and Sutherland, P. G. 1975, *Ap. J.*, **196**, 51.
Scargle, J. D. 1969, *Ap. J.*, **156**, 401.
———. 1971, *Nature Phys. Sci.*, **230**, 37.
Scharlemann, E. T. 1979, in *Particle Acceleration Mechanisms in Astrophysics*, ed. J. Arons, C. E. Max, and C. F. McKee (New York: American Institute of Physics), p. 373.
Scharlemann, E. T., Arons, J., and Fawley, W. M. 1978, *Ap. J.*, **222**, 297.
Scharlemann, E. T., and Wagoner, R. V. 1973, *Ap. J.*, **182**, 951.
Schattenburg, M. L., Canizares, C. R., Berg, C. J., Clark, G. W., Markert, T. H., and Winkler, P. F. 1980, *Ap. J.* (*Letters*), **241**, L151.
Schmidt, G. D., Angel, J. R. P., and Beaver, E. A. 1979, *Ap. J.*, **227**, 106.
Shklovsky, I. S. 1968, *Supernovae* (New York: Wiley), p. 327.
Staubert, R., Kendzierra, E., Trumper, T., Reppin, C., Horrman, J. A., Pounds, K. A., Giles, A. B., and Morrison, L. V. 1975, *Ap. J.* (*Letters*), **201**, L15.
Sturrock, P. 1971, *Ap. J.*, **164**, 529.
Swinbank, E. 1980, *M.N.R.A.S.*, **193**, 451.
Swinbank, E., and Pooley, G. 1979, *M.N.R.A.S.*, **186**, 775.
Toor, A., Palmieri, T. M., and Seward, F. D. 1976, *Ap. J.*, **207**, 96.
Trimble, V. 1968, *A.J.*, **73**, 535.
———. 1971, in *IAU Symposium 46*, *The Crab Nebula*, ed. R. Davies and F. Smith (Dordrecht: Reidel), p. 12.
Trimble, V., and Rees, M. 1970, *Ap. Letters*, **5**, 93.
van den Bergh, S. 1970, *Ap. J.* (*Letters*), **160**, L27.
Weber, E. J., and Davis, L., Jr. 1967, *Ap. J.*, **148**, 217.
Weiler, K. W. 1973, *Astr. Ap.*, **26**, 403.
Weiler, K. W., and Panagia, N. 1978, *Astr. Ap.*, **70**, 419.
Weiler, K. W., and Wilson, A. S. 1977, *Astr. Ap.*, **58**, 17.
Weisskopf, M. C., Cohen, C. G., Kestenbaum, H. L., Long, K. S., Novick, R., and Wolff, R. S. 1976, *Ap. J.* (*Letters*), **208**, L125.
Wilson, A. S. 1972, *M.N.R.A.S.*, **157**, 229.
Wilson, A. S., and Weiler, K. W. 1982, *Nature*, **300**, 155.
Wilson, D. B., and Rees, M. J. 1978, *M.N.R.A.S.*, **185**, 297.
Wolff, R. S., Kestenbaum, H. L., Ku, W., and Novick, R. 1975, *Ap. J.* (*Letters*), **202**, L15.
Woltjer, L. 1957, *Bull. Astr. Inst. Netherlands*, **13**, 301.
Wright, M. C. H., and Forster, J. R. 1980, *Ap. J.*, **239**, 873.
Wyckoff, S., and Murray, C. A. 1977, *M.N.R.A.S.*, **180**, 717.
Wyckoff, S., Wehinger, P. A., Fosbury, R., and McMullan, D. 1976, *Ap. J.*, **206**, 254.

F. V. Coroniti: Departments of Physics and Astronomy, University of California, Los Angeles, CA 90024

C. F. Kennel: Department of Physics, University of California, Los Angeles, CA 90024